Nanoscale Advances

ROYAL SOCIETY OF CHEMISTRY

REVIEW

View Article Online
View Journal | View Issue

Check for updates

Cite this: *Nanoscale Adv.*, 2025, **7**, 3941

Synthesis methods, structure, and recent trends of ZIF-8-based materials in the biomedical field†

Thuan Van Tran, *[a] Hoang Huy Dang,[a] Huy Nguyen,[a] Ngoan Thi Thao Nguyen,[ab] Dai Hai Nguyen [c] and Thuy Thi Thanh Nguyen*[b]

Received 5th December 2024
Accepted 19th April 2025

DOI: 10.1039/d4na01015a

rsc.li/nanoscale-advances

Zeolitic imidazolate framework-8 (ZIF-8) is a highly porous material with remarkable structural properties and high drug-loading capacity, and hence this material presents as an exceptional candidate for advanced drug delivery systems. Herein, we comprehensively review the recent developments in ZIF-8 synthesis techniques and critically discuss innovative approaches such as the use of green solvents and advanced methods such as microwave- and ultrasound-assisted syntheses. The multifunctional applications of ZIF-8-based biomaterials in biomedical engineering are critically explored with their pivotal roles in antibacterial and anticancer therapies, drug delivery systems, bone tissue engineering, and diagnostic platforms such as biosensing and bioimaging. The present review also clarifies some innovations of ZIF-8-based materials in pH-sensitive and glucose-responsive drug delivery systems and scaffolds for bone regeneration. Despite these promising advancements, we analyze critical concerns, such as the release of Zn(II) ions, potential cytotoxicity, and biocompatibility challenges, which remain significant hurdles to the broader adoption of ZIF-8. Addressing these outlined challenges may be necessary in realizing the potential of ZIF-8 in biomedical applications.

Open Access Article. Published on 27 Mei 2025. Downloaded on 02/06/2026 13:51:38.
This article is licensed under a Creative Commons Attribution-NonCommercial 3.0 Unported Licence.

1. Introduction

Zeolitic imidazolate frameworks (ZIFs), a subclass of metal–organic frameworks, possess exceptional properties, such as thermal and chemical stability, high porosity, and tunable surface chemistry.[1,2] ZIF-8, a prototypical member of the ZIF family, is composed of zinc clusters (Zn^{2+}) and imidazolate linkers (2-Hmim). This material has a chemical formula of Zn(2-Hmim)$_2$, having the same topology as sodalite-type zeolites with a Zn-[2-Hmim]-Zn angle of 145° and a pore aperture of 3.4 Å.[3] Structurally, each building unit of ZIF-8 is a Zn(2-Hmim)$_2$ tetrahedron, while the crystal structure exhibits a rhombic dodecahedral or cubic shape.[4] These structural characteristics endow ZIF-8 with high flexibility and multifunctionality, recently offering key benefits for application in lithium sulfur batteries,[5] electrocatalysis,[6] as nanocomposite scaffolds in wound healing,[7] pH-responsive drug delivery systems,[8] perovskite photovoltaics,[9] and in water treatment.[10] As a result, efforts to broaden its scope in biomedical engineering have attracted great attention.

Biomedical engineering leverages interdisciplinary approaches between materials and medical sciences to solve healthcare problems, and ZIF-8 materials hold significant advantages in this domain.[11] Indeed, the pH-sensitive drug release of ZIF-8 is advantageous for applications such as cancer treatment, where acidic tumor microenvironments enable precise drug release while minimizing off-target effects.[12] Possessing highly porous and versatile structure, ZIF-8-based carriers have a high drug-loading capacity and hence can be incorporated with diverse therapeutic agents for targeted drug delivery systems.[13] Another promising avenue for ZIF-8 is in tissue engineering, wherein ZIF-8-based scaffolds are often combined with biopolymers or loaded with bioactive molecules to promote osteogenesis, angiogenesis, and bone integration.[14] These systems not only facilitate the healing of critical-sized bone defects but also exhibit antibacterial properties, an essential feature for preventing infections.[15] Importantly, the pore structure and surface chemistry of ZIF-8 can be still modulated *via* functionalization, enabling tailored solutions for specific medical applications.[16]

This review systematically discusses recent developments in ZIF-8 synthesis methods and critically examines the multifunctional applications of ZIF-8-based materials in biomedical engineering with a focus on their emerging roles in antibacterial therapy, anticancer therapy, drug delivery, bone tissue engineering, biosensing and bioimaging for diagnostic systems

[a]*Institute of Applied Technology and Sustainable Development, Nguyen Tat Thanh University, 298-300A Nguyen Tat Thanh, District 4, Ho Chi Minh City 755414, Vietnam. E-mail: tranvt@ntt.edu.vn*

[b]*Nong Lam University Ho Chi Minh City, Ho Chi Minh City 700000, Vietnam. E-mail: nguyenthanhthuy@hcmuaf.edu.vn*

[c]*Institute of Advanced Technology, Vietnam Academy of Science and Technology, 1B TL29 Street, Thanh Loc Ward, District 12, Ho Chi Minh City, 700000, Vietnam*

† Electronic supplementary information (ESI) available. See DOI: https://doi.org/10.1039/d4na01015a

© 2025 The Author(s). Published by the Royal Society of Chemistry

Open Access Article. Published on 27 Mei 2025. Downloaded on 02/06/2026 13:51:38.
This article is licensed under a Creative Commons Attribution-NonCommercial 3.0 Unported Licence.

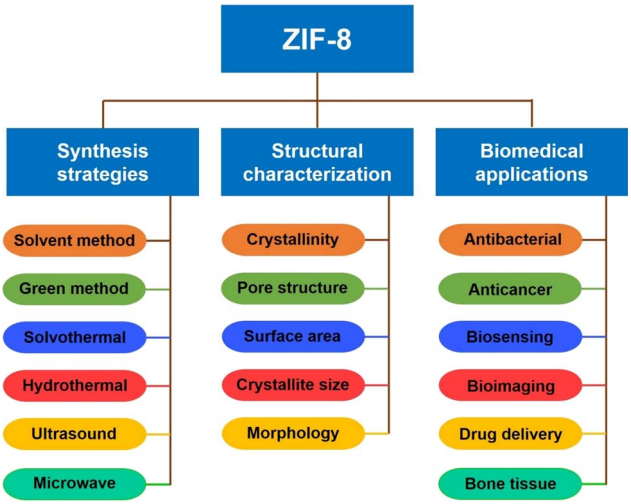

Fig. 1 A schematic flowchart to show the synthesis strategies, structure characterization, and biomedical applications of ZIF-8 materials.

(Fig. 1). Unlike previous reviews that focus on either the general properties of ZIFs or their applications in a specific domain, we expect this work to bridge multiple biomedical disciplines to provide a holistic perspective on the versatility of ZIF-8. The present review discusses the latest advancements in pH-sensitive and glucose-responsive drug delivery systems, innovative scaffolds for bone regeneration, and theranostic platforms integrating diagnostic and therapeutic functionalities. This review also recommends future research studies to address current limitations, such as toxicity and scalability. Alongside future prospects, this review supplies novel insights into the design and development of next-generation ZIF-8-based biomedical materials, making them an indispensable resource in the field.

2. Synthesis strategies

2.1. Background

ZIF-8 is composed of Zn clusters and imidazolate ligands; thus, Zn^{2+} and 2-methylimidazole (2-Hmim) are two major precursors (Table S1†). Several studies have reported that ZnO can also be used as an alternative to Zn^{2+} salt.[17–20] Since water is a by-product of the process, this strategy is more inexpensive and sustainable than the ones used, Zn^{2+} and 2-methylimidazole.[17] However, the growth of ZIF-8 from ZnO may require several specific conditions. For example, ZIF-8 crystals are grown on cotton fibers as a "scaffold",[21] on Al_2O_3/ZnO hollow fibers,[19] on a polyacrylonitrile support *via* magnetron sputtering,[20] or under the exposure of both ultrasound and microwave irradiations.[17]

The mole ratio between Zn^{2+} and 2-methylimidazole (2-Hmim) is a key factor since it is often associated with yield, purity, and characteristic of obtained ZIF-8 materials.[22] Table S1† reveals that this ratio ranges from 1 : 2 to 1 : 8. Some studies have reported the mole of 2-Hmim can be higher than that of Zn^{2+}.[23,24] A larger mole ratio of 2-Hmim can lead to higher yields and complete reactions. However, 2-Hmim is an expensive linker chemical, resulting in the fact that the total production cost is more likely to be very high. Unreacted 2-Hmim molecules can get stuck inside the pores of ZIF-8, decreasing the surface area of the resulting materials. An excessive amount of 2-Hmim when released into water sources without proper treatment can also become a new pollutant or can be a toxin to microorganisms and aquatic species.[25] Consequently, optimizing the mole ratio between Zn^{2+} and 2-Hmim in various ZIF-8 synthesis methods should be investigated.

For synthesis of MOFs, solvents and additives play a vital role in the nucleation, crystal growth, crystallite size, morphology control, surface area, topology, and stability.[26] The commonly used solvents for ZIF-8 preparation are H_2O, methanol (MeOH), and *N*,*N*-dimethylformamide (DMF). In some cases, a mixed solvent can be a feasible solution to curb the use of harmful solvents such as DMF, MeOH, *etc.*[27] Triethylamine [TEA, $N(CH_2CH_3)_3$] is often added as a basic additive to facilitate the deprotonation of 2-Hmim, accelerating the reaction rate between Zn^{2+} and 2-Hmim to form new frameworks.[28] Although TEA is toxic and flammable, the addition of this reagent into the reaction solution offers undebatable advantages, *i.e.*, minimizing the amount of 2-Hmim and reducing the synthesis duration.[28] The additives can be butylamine, polyamine, and sodium hydroxide.

There are currently many methods used for synthesis of ZIF-8, such as the solvent method, water-based method, solvothermal method, hydrothermal method, ultrasound-assisted method, microwave-assisted method, and mechanochemical method. Among them, the water-based method is preferable since this method uses water as the main solvent, while the mechanochemical method often does not use or only uses a small amount of solvents. Ultrasound-assisted and microwave-assisted methods offer many advantages such as the rapid synthesis process. However, these methods can present several shortcomings, which are clarified in the next subsections.

2.2. Solvent method

In this method, polar solvents such as MeOH or mixed solvents such as ammonium hydroxide (NH_4OH) in water are often used (Table S1†). Because these solvents have low boiling points, ZIF-8 synthesis is preferred at room temperature (RT). Kiwaan *et al.*[27] used a mixed solvent of H_2O and NH_4OH (1 : 7 by vol.) for the synthesis of ZIF-8 for 10 min. However, the surface area of ZIF-8 synthesized by the solvent method was relatively low due to the low dissolution of 2-Hmim in NH_4OH/H_2O solvent. In this case, the residual organic linkers still remain trapped in the pores of as-obtained ZIF-8. Thus, the use of this mixed solvent for ZIF-8 synthesis was rarely reported in the solvent method.

MeOH was widely used because the resulting ZIF-8 exhibited a higher surface area (1291–1932 $m^2\ g^{-1}$). This solvent can easily dissolve both Zn^{2+} and 2-Hmim, facilitating the reaction between them at room temperature. According to Table S1,† as the Zn^{2+} to 2-HMim ratio increased (1 : 8–1 : 3.5), the reaction time tends to increase (1–24 h). An excessive amount of ligand accelerates the nucleation and crystal growth of ZIF-8. In these

© 2025 The Author(s). Published by the Royal Society of Chemistry

Open Access Article. Published on 27 Mei 2025. Downloaded on 02/06/2026 13:51:38.
This article is licensed under a Creative Commons Attribution-NonCommercial 3.0 Unported Licence.

cases, the kinetic rate of ZIF-8 synthesis in MeOH media can be controlled by the mole ratio of reagents. Meanwhile, Cheng *et al.*[29] increased both the Zn^{2+} to 2-HMim ratio (1 : 8) and reaction time (48 h) to produce ZIF-8 in MeOH at room temperature. However, the surface area did not increase significantly (1115.2 m^2 g^{-1}), suggesting that a prolonged reaction time may affect the porosity of ZIF-8. The highest surface area of ZIF-8 synthesized by the solvent method was 1932 m^2 g^{-1} at a high Zn^{2+}/2-HMim ratio (1 : 7) and low reaction time (1 h).[30] There is a disadvantage of the solvent method using methanol as solvent, that is high toxicity. The recovery of methanol and residual Zn metal from the mixture after ZIF-8 synthesis is also a costly and time-consuming process.

2.3. Water-based method

Water is a non-expensive, highly polar, and clean solvent for material synthesis. However, several organic reagents limitedly dissolve in water, reducing the total production yield. In such cases, a mixed solvent of water and an organic solvent (*e.g.*, *t*-BuOH, MeOH, DMF) is more appropriate. The use of water as a solvent for ZIF-8 synthesis offers several advantages. First, water can be used to replace some toxic or expensive solvents such as MeOH, and DMF. Second, the aqueous reaction is often carried out at room temperature. However, the amount of 2-Hmim is largely high at a 1 : 70 ratio,[31] or a prolonged reaction time (48 h) is required.[29] Moreover, the surface area of ZIF-8 obtained by this method is lower than that of ZIF-8 obtained by the solvent method.[29]

2.4. Solvothermal method

Over the past decades, hydrothermal synthesis has been applied to synthesize zeolites, nanoparticles, polymers, porous metal–organic or inorganic–organic hybrid materials.[32] The solvothermal synthesis normally takes place inside a Teflon-lined steel autoclave to obtain a temperature higher than the boiling point of the used solvents. Moreover, the pressure of this process is higher than the atmospheric pressure (1.0 atm, 760 mm Hg). During the hydrothermal process, the temperature of solvothermal reactions can reach up to 250 °C.[33] The major safety concern is that the reactants need to be dissolved under high temperature and pressure conditions; it is therefore necessary to be equipped with various protection accessories.

Different single solvents can be used for the solvothermal preparation of ZIF-8-based materials.[13] Mixed solvents are also used, *i.e.*, either mixture of organic solvents, such as methanol (MeOH), ethanol (EtOH), acetonitrile (MeCN), *N*,*N*-dimethylformamide (DMF), and *N*,*N*-diethylformamide (DEF) or mixture of organic solvents and inorganic solvents, such as water.[34] According to Table S1,† DMF serves as a common solvent since it can easily dissolve the organic ligand 2-Hmim and zinc salts. DMF also offers great advantages such as high boiling point and high polarity, which are necessary for the solvothermal process. Considering DMF as a solvent, the temperature and time for the solvothermal synthesis of ZIF-8 often fall in the range 100–140 °C and 18–24 h, respectively. The synthesis conditions at these temperatures and time are adequate for crystal growth during the solvothermal process.[13,27,34]

2.5. Hydrothermal method

The hydrothermal method is a kind of wet chemical method to produce nanomaterials such as metal oxides and spinel ferrites.[35,36] Typically, precursors are mixed together using an aqueous solution and heated at a high temperature (200–300 °C) to reach a high vapor pressure.[35] High temperature and pressure conditions allow precursors to react rapidly. Same as solvothermal methods, hydrothermal reactions are often carried out in specially sealed vessels or high-pressure resistant autoclaves.[13,37]

Synthesis of ZIF-8 by the hydrothermal method has been reported in the past studies. For example, Li *et al.*[38] hydrothermally synthesized ZIF-8 at 120 °C for 6 h using H_2O as a solvent. However, the Zn^{2+} to 2-Hmim mole ratio was reported to be up to 1 : 57, resulting in a very large amount of residual 2-Hmim as a toxic waste. By adding TEA as an additive, Butova *et al.*[28] reduced this ratio to 1 : 2 for the hydrothermal synthesis of ZIF-8. This materials had an exceptionally high surface area of 1340 m^2 g^{-1}. The reaction duration was quite long (24 h), which can be a weakness of this method. Malekmohammadi *et al.*[39] addressed these disadvantages (high temperature and long duration) by using a mixed solvent of MeOH and H_2O with a ratio of 2 : 15. Consequently, the formed ZIF-8 offered a very high yield of 97% at 25 °C for 20 h.

2.6. Ultrasound-assisted method

Compared with conventional synthesis methods (hydrothermal and solvothermal), non-conventional microwave-assisted methods (sonochemistry) bring special reaction conditions, *i.e.*, supply high energy for a very short time, and enhance the chemical activity of reactants.[40,41] This technique uses high-frequency waves (20–1000 kHz) to exert acoustic cavitation, which leads to the formation, expansion, and flash collapse of bubbles or "hot spots".[40] Therefore, hot spots receive extremely high temperature (5000 °C) and pressure (1000 atm), and boost the rate of reactions.

Ultrasound-assisted ZIF-8 synthesis is mainly conducted in MeOH or H_2O at room temperature and with a Zn^{2+}/2-Hmim ratio from 1 : 2 to 1 : 70 (Table S1†). For instance, Nalesso *et al.*[42] surveyed the effect of various micromixing rates, ultrasound frequencies, calorimetric powers, and ultrasound times on the formation of ZIF-8 nanocrystals using H_2O as the solvent. The authors concluded that frequency and power of sonication had a negligible impact on the crystal properties such as crystallinity, purity and yield. Interestingly, ZIF-8 nanocrystals were produced with a small size (80 nm) within only 5 s of sonication (Fig. 2a and b). However, sonication by shockwaves resulted in a decreased surface area of ZIF-8. The use of surfactant aids the nucleation and crystal growth, augmenting the production of ZIF-8. Indeed, Luan Tran *et al.*[44] used Pluronic P-123 (a copolymer) as a surfactant to reduce the time for the ultrasound-assisted synthesis of ZIF-8 from 10 min to 1 min. Cho *et al.*[43] compared the production yield of ZIF-8 between sonochemical

Open Access Article. Published on 27 Mei 2025. Downloaded on 02/06/2026 13:51:38.
This article is licensed under a Creative Commons Attribution-NonCommercial 3.0 Unported Licence.

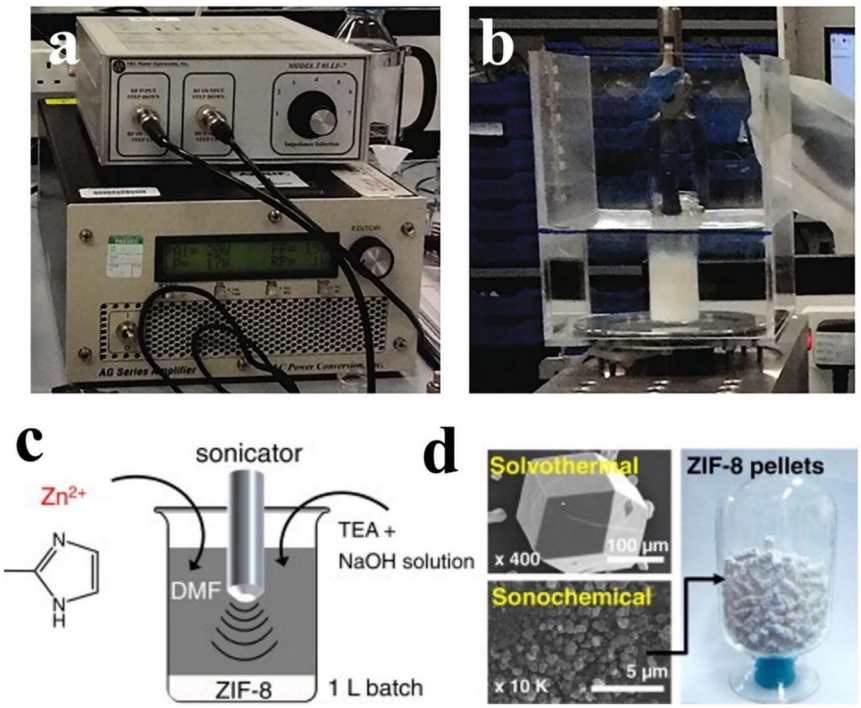

Fig. 2 Ultrasonic generator equipment with a step-up transformer (a) and the glass vial reactor for ZIF-8 placed in an ultrasonic bath (b). This figure has been reproduced from ref. 42 with permission from Elsevier, copyright 2021. Ultrasound-assisted synthesis of ZIF-8 using TEA and NaOH additives (c) and morphological comparison of ZIF-8 between solvothermal and sonochemical methods (d). This figure has been reproduced from ref. 43 with permission from Elsevier, copyright 2013.

and solvothermal methods. The space-time yield (STY, kg per m^3 per day) results showed that the STY of the former (~1200 times) was higher than that of the latter. Moreover, the crystallite size of ZIF-8 prepared by the sonochemical method was considerably smaller than that of ZIF-8 prepared by solvothermal methods (Fig. 1c and d).

2.7. Microwave-assisted method

Microwave heating is one of the widely used non-conventional methods for pyrolytic conversion of biomass into biochars, bio-oils and biogases,[45–47] electrification of the clinker for cement manufacturing,[48] food processing,[49] and nanomaterial synthesis.[50,51] In this method, the electromagnetic field with a frequency from 300 MHz to 300 GHz is induced to rotate dipolar molecules instantaneously.[52,53] This process gives rise to heating energy from collision among molecules. Microwaves are irradiated from the inside to outside so that the sample was uniformly heated (Fig. 3).

The interaction degree between molecules and the electromagnetic field significantly depends on the dielectric properties.[55] As a result, the selection of solvent plays a key role in the formation of nucleation, crystal growth and MOF particles, thereby reducing the synthetic duration to a few minutes or few hours.[56] Common solvents, including MeOH, DMF, mixed MeOH/DMF, and so forth, are used for ZIF-8 synthesis (Table S1†). Similar to conventional and non-conventional methods, TEA is often added in the solvent to assist the deprotonation of 2-Hmim. However, several main disadvantages of microwave heating are indicated, such as limited scalability, well-equipped and complex instruments to protect operators from microwave irradiation, difficulty in reaction temperature control, and heavy energy consumption.[52]

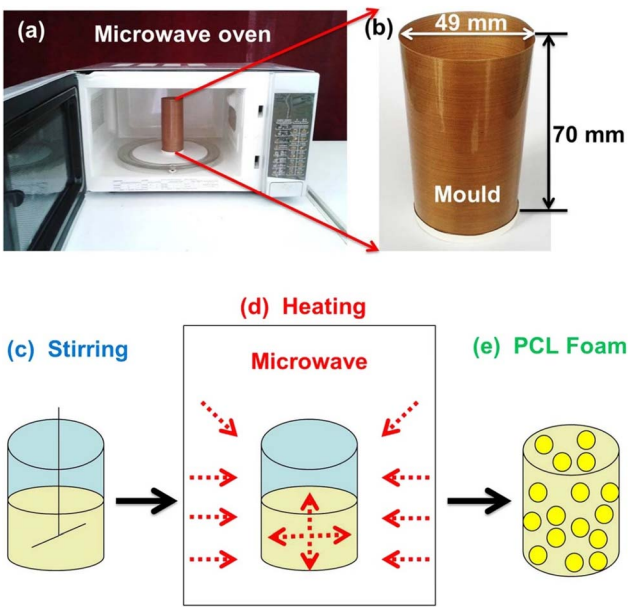

Fig. 3 A real photograph of a microwave oven (a) and a cylindrical mould reactor (b). The processes of stirring (c), microwave heating (d) and the formation of a biodegradable shape memory crosslinked-polycaprolactone (PCL) foam (e). This figure has been reproduced from ref. 54 with permission from Springer Nature copyright 2015.

© 2025 The Author(s). Published by the Royal Society of Chemistry

Open Access Article. Published on 27 Mei 2025. Downloaded on 02/06/2026 13:51:38.
This article is licensed under a Creative Commons Attribution-NonCommercial 3.0 Unported Licence.

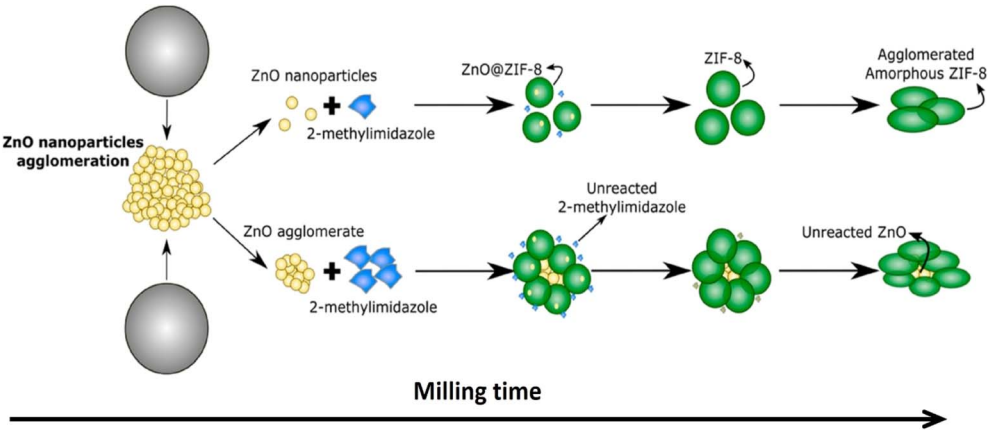

Fig. 4 The reaction between ZnO nanoparticles and 2-methylimidazole during dry milling to produce ZIF-8. This figure has been reproduced from ref. 57 with permission from Royal Society of Chemistry, copyright 2020.

2.8. Mechanochemical method

Mechanochemistry has been used to produce ZIF-8 through the use of mechanical forces (*e.g.*, grinding and milling) to initiate chemical reactions.[57] In this method, agglomerated ZnO particles are milled into ZnO nanoparticles, which act as a precursor to react with 2-methylimidazole without the use of solvent (Fig. 4). The mechanochemical energy exerts pressure on the surface of ZnO nanoparticles to generate a local heating source and a high-entropy system for the synthesis of ZIF-8.[58] The mechanochemical method is considered a solvent-free and toxic chemical-free method, hence this method may be a potentially greener alternative to traditional chemical synthesis methods.[59] However, several disadvantages should be indicated that high energy consumption and mechanical equipment may be required for milling or grinding ZnO particles to reduce their size to a nano-scale.

Taheri *et al.*[57] conducted a one-step mechanochemical processing of ZnO nanoparticles and 2-methylimidazole for 12 h of milling. By fixing the ball-to-powder mass ratio (10 : 1) and controlling the stoichiometric mixture of two precursors, ZIF-8 nanocrystals were formed with a conversion yield of 100% based on ZnO nanopowder. ZIF-8 had a size of about 80 nm, good dispersion, and a surface area of up to 1885 $m^2 g^{-1}$. Wei *et al.*[60] successfully encapsulated enzymes in ZIF-8 to form biocomposites for enhancing enzymatic biological activities. In this study, the mechanochemical processing of ZnO and 2-methylimidazole was carried out for only 2.5 min and of as-obtained ZIF-8 and enzymes for another 2.5 min. The main findings indicated that the mechanochemical method was used to not only create ZIF-8 rapidly but also encapsulate enzymes effectively.

2.9. Large-scale synthesis

The large-scale production of uniform, narrow-size, and highly crystalline ZIF-8 has been conducted by Kim *et al.*[61] In this study, the authors used a 2 L water batch experiment at room temperature without surfactants to obtain a ZIF-8 powder mass of 55 g (nearly 92% in yield). The ZIF-8 particle sizes were from 500 to 520 nm. The synthesis procedure was considered safe due to the use of deionized water instead of an organic solvent. However, the production mass of ZIF-8 by this protocol was still relatively small.

Through an intermediate phase transformation strategy, Deacon *et al.*[62] produced up to 1 kg of nano-scale ZIF-8 on a pilot scale with a production yield of 81% and a space-time yield of 25 kg per m^3 per day. Different from the synthesis procedure reported by Kim *et al.*,[61] these researchers first synthesized ZIF-L on a large scale using 2.22 kg of 2-methylimidazole and 1.3 kg of zinc nitrate hexahydrate, then transformed ZIF-L into ZIF-8 by dispersing in 2-propanol at 80 °C for two days. Large-scale synthesized ZIF-8 through the transformation route possessed an outstanding surface area (S_{BET}: 1745 $m^2 g^{-1}$), which was higher than that of ZIF-8 synthesized using the original route. These findings suggest a promising strategy to synthesize ZIF-8 on a large scale.

3. Structural characterization of ZIF-8

3.1. Crystal structure

Constructed from one Zn^{2+} site and four imidazolate linkers, the basic ZIF-8 structure includes two flexible gates, *e.g.*, a four-membered ring and a six-membered ring, forming a tetrahedral topology (ZnN_4).[63] The six-membered ring (diameter, 3.4 Å) is the most typical configuration for ZIF-8 since the guest molecules can access this gate (Fig. 5). This departure leads to the best CO_2/CH_4 separation performance of ZIF-8.[64] Based on XRD analysis, ZIF-8 has main peaks at 7.3 (011), 10.4 (002), 12.7° (112), 14.7° (002), 16.4° (013), and 18° (022), suggesting that ZIF-8 exhibits a highly crystalline structure.[65]

The effect of *in situ* or post-synthetic modification on the crystal structure of ZIF-8 was studied. Take *in situ* synthesis for example, by adding a cationic polyelectrolyte modifier such as poly(diallyldimethylammonium chloride) in a mixture of Zn^{2+} and 2-Hmim in water, Zhang *et al.*[65] observed that the intensity of main peaks tended to decrease considerably and even disappeared in the (002) plane. This outcome could be attributable to the crystal defects and the formation of a dense dia-framework. Similarly, the addition of Zn^{2+} and Fe^{3+} that leads

Open Access Article. Published on 27 Mei 2025. Downloaded on 02/06/2026 13:51:38.
This article is licensed under a Creative Commons Attribution-NonCommercial 3.0 Unported Licence.

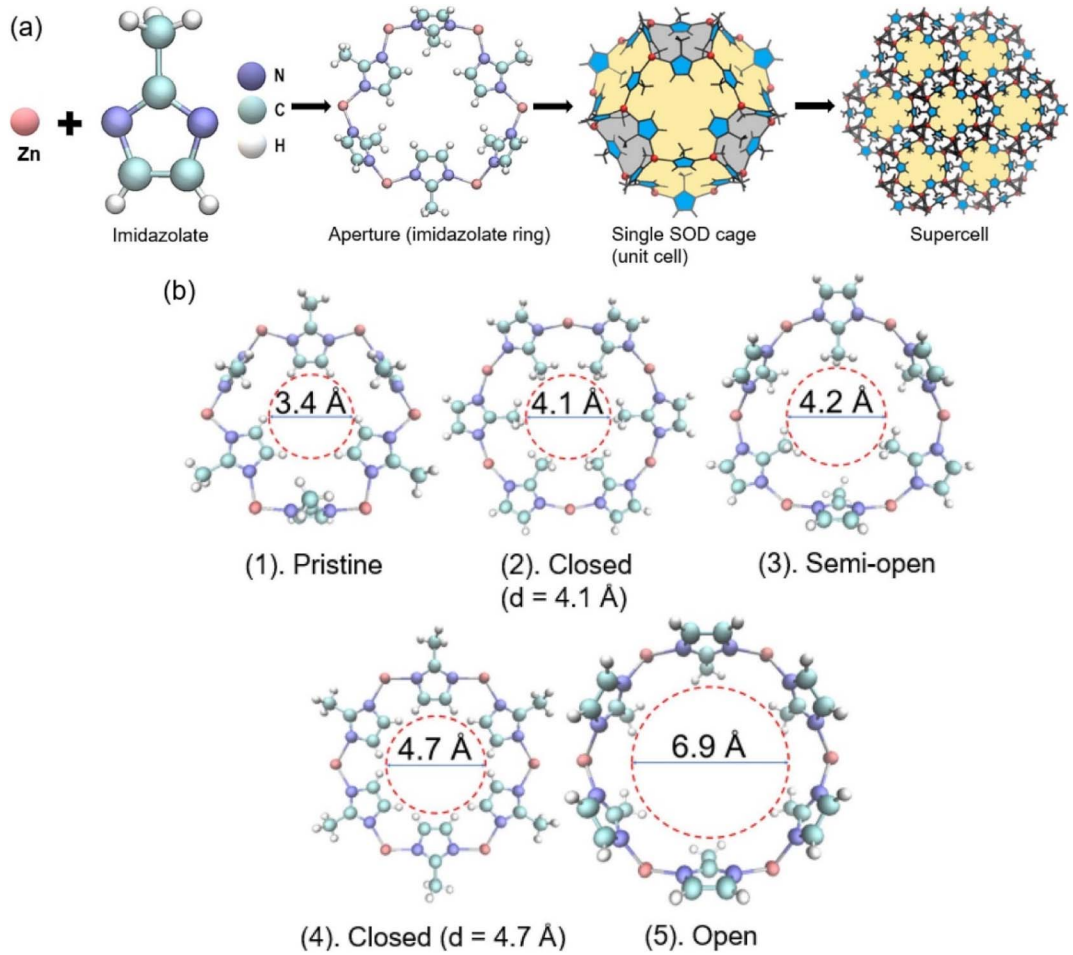

Fig. 5 (a) The structural and topological simulation of ZIF-8 and (b) five different aperture structures of ZIF-8. This figure has been reproduced from ref. 64 with permission from Elsevier, copyright 2021.

to the formation of $ZnFe_2O_4$ nanoparticles into ZIF-8 particles dispersed in ethylene glycol, can decrease the crystallinity of ZIF-8.[66] A minor peak shift was also observed for $ZnFe_2O_4$/ZIF-8 compared with ZIF-8, associated with interactions such as electrostatic and magnetic forces.

The effect of solvent on the crystal structure of ZIF-8 was also reported. Indeed, Tezerjani *et al.*[67] observed the alteration in the ZIF-8 structure synthesized using three different solvents, including H_2O, MeOH, and DMF. Compared with the use of MeOH, these authors found that the synthesis of ZIF-8 using DMF solvent resulted in an increase in crystallinity and a decrease in the crystallite size in all three synthesis methods: mixing, solvothermal and sonochemical. For the synthesized ZIF-8 in water, the presence of an amorphous phase along with the divergence in the position of main diffraction peaks at (001), (002), (112), and (222) has been observed. These findings reflected the heavy dependence of crystal structure of ZIF-8 on the solvent.

3.2. Pore structure

Solvent plays a vital role in the pore structure among various factors. Most ZIF-8 crystals were synthesized using organic solvents such as MDF, MeOH, and TEA (Table S1†). Organic solvents enhance the mixing and contact between Zn^{2+} and 2-HMim, accelerating the nucleation and crystal growth. The structure of ZIF-8 in these cases was reported to be highly porous, including microporous and mesoporous. For example, Santoso *et al.*[68] found that the pore volume of ZIF-8 synthesized in two solvents including DMF and 2% AcOH in H_2O (TEA as a directing agent) was 0.54 $cm^3\ g^{-1}$ and 0.43 $cm^3\ g^{-1}$, respectively. Moreover, the pore sizes were measured as 2.1 nm and 3.2 nm, respectively, indicating that solvent profoundly affected the pore structure of ZIF-8.

Cheng *et al.*[29] investigated the effect of crystal growth rate on the pore volume of ZIF-8 samples. In this study, ZIF-8 crystals were grown in three solvents including NH_4OH in water (1 : 1.26 by vol.) for 10 min, MeOH for 24 h, and H_2O for 24 h to form ZIF-8-A, ZIF-8-M, and ZIF-8-W, respectively. Although the reaction time of ZIF-8 synthesis in each solvent was considerably different, the total pore volume of ZIF-8 samples insignificantly changed between 0.68 for ZIF-8-M and 0.54 $cm^3\ g^{-1}$ for ZIF-8-A and ZIF-8-W. Along with a minor change in the surface area, the authors suggested that the microporous structure of ZIF-8 relied

© 2025 The Author(s). Published by the Royal Society of Chemistry

Open Access Article. Published on 27 Mei 2025. Downloaded on 02/06/2026 13:51:38.
This article is licensed under a Creative Commons Attribution-NonCommercial 3.0 Unported Licence.

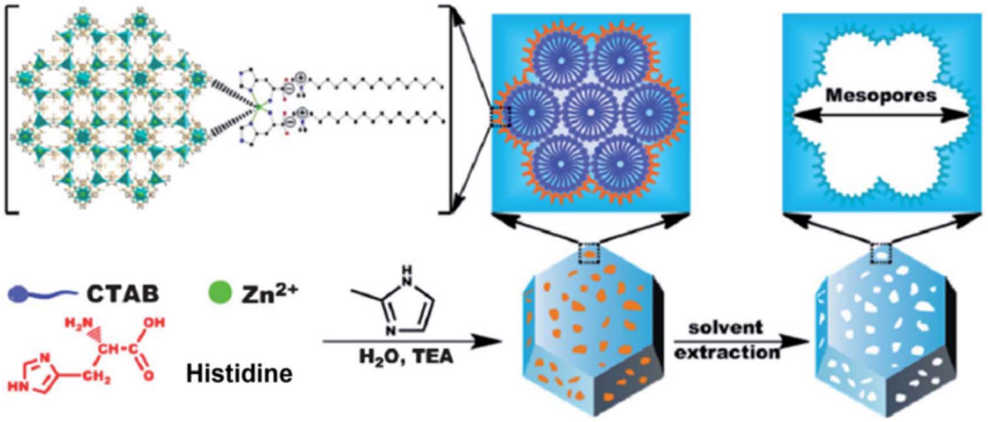

Fig. 6 Possible role of CTAB surfactant and L-histidine co-template in the formation of mesoporous ZIF-8 crystals. This figure has been reproduced from ref. 69 with permission from Royal Society of Chemistry, copyright 2014.

negligibly on the growth rate, but relied heavily on solvents and other factors.

The use of H_2O as a solvent was reported in some cases but often required a very high ratio of 2-HMim.[29,31,38,42] This approach is more likely to lead to lower porosity and yield of the resulting ZIF-8. Wu *et al.*[69] reported the addition of cetyltrimethylammonium bromide (CTAB) surfactant into H_2O solvent to form mesoporous ZIF-8. The authors suggested that only CTAB as a single template did not foster the formation of mesopores because Zn^{2+} was entrapped in the hydrophilic outer layer. When L-histidine was added, it acted as a co-template that helps to create a stable electrostatic interaction between CTAB micelles and Zn^{2+} ions (Fig. 6). After solvent extraction, ZIF-8 obtained a mesoporous structure. Additionally, other synthesis strategies including host–guest chemistry, template, post-synthetic ion exchange, core–shell structure and precursor support can affect the pore structure of ZIF-8 and its derivatives but have been uncommonly reported.[6]

3.3. Surface area

Surface areas of ZIF-8 are often varied, and dependent on many factors such as the synthesis method, the solvent or mixed solvent, and the Zn^{2+} to 2-Hmim ratio (Table S1†). Overall, the solvent synthesis using MeOH often brings high surface areas of ZIF-8, from 1000 to 2000 $m^2\ g^{-1}$. Similarly, the solvothermal method using DMF results in a relatively high surface area of ZIF-8, at larger than 900 $m^2\ g^{-1}$. The sonochemical method may be a preferable and safe approach to synthesize ZIF-8 with high surface areas (891–2000 $m^2\ g^{-1}$). By contrast, it should be difficult to control the surface area of ZIF-8 through the microwave-assisted method. This drawback can be due to very fast heating of microwave irradiation affecting the nucleation and crystal growth. Importantly, unreacted 2-Hmim can be trapped in pores or the 6-membered ring gate of ZIF-8, leading to a considerable reduction in its surface area.[70] Finally, considering the high surface area, green synthesis of ZIF-8 using H_2O at room temperature can have great potential for commercialization.[29,31]

The effect of solvent on the surface area of ZIF-8 was studied in earlier literature. For instance, Kiwaan *et al.*[27] synthesized ZIF-8 crystals by using ammonium hydroxide in water. They mixed $Zn(NO_3)_2 \cdot 6H_2O$ salt with 2-methylimidazole and then dissolved the obtained mixture in ammonium hydroxide solution to initiate ZIF-8 crystallization under stirring. The results showed that the synthesized ZIF-8 material possessed a moderate surface area of 495.19 $m^2\ g^{-1}$ and a pore volume of 0.28 $cm^3\ g^{-1}$. However, this method has some limitations such as time consuming and poor porosity of resulting ZIF-8.

By changing the solvent to MeOH, the surface area of ZIF-8 can be enhanced. Indeed, Xu *et al.*[30] achieved a very high surface area (1932 $m^2\ g^{-1}$) for ZIF-8 synthesized using MeOH solvent at room temperature for 12 h. Ostad *et al.*[71] compared the effect of different solvents on the surface area of ZIF-8, which followed the order: ammonia (1568 $m^2\ g^{-1}$) > H_2O/EtOH (1 : 8, by vol%) (1356 $m^2\ g^{-1}$) > MeOH (1333 $m^2\ g^{-1}$). Upon refluxing ammonia-based as-synthesized ZIF-8 in MeOH at 70 °C for 1 day, the authors observed a slight increase (about 13%) in surface area. This improvement can be attributable to the solvent extraction of ammonia from the pores of ZIF-8 when immersed in MeOH.

3.4. Crystallite size

The effect of the type of solvent, surfactant, Zn^{2+}/2-HMim, and synthesis method on ZIF-8 crystallite size has been studied (Table S1†). For example, Cheng *et al.*[29] reported a very large size of ZIF-8 (~1000 nm) synthesized *via* the solvent method using a mixture of H_2O and NH_4OH at a volume ratio of 1 : 1.26. By changing this ratio up to 1 : 7 under the same conditions, Kiwaan *et al.*[27] obtained ZIF-8 nanocrystals with a very low average size (38.1 nm). The higher concentration of NH_4OH increases the pH, which affects the reaction rate between of Zn^{2+} and 2-HMim in basic solutions. Similarly, the solvent seemed to be a major factor that controls ZIF-8 crystallite size in the ultrasonication method.[44] The authors replaced NH_4OH with H_2O and used Pluronic P-123 as a surfactant. As a result, the ZIF-8 size was found to decrease from 2000 nm to 50–

Open Access Article. Published on 27 Mei 2025. Downloaded on 02/06/2026 13:51:38.
This article is licensed under a Creative Commons Attribution-NonCommercial 3.0 Unported Licence.

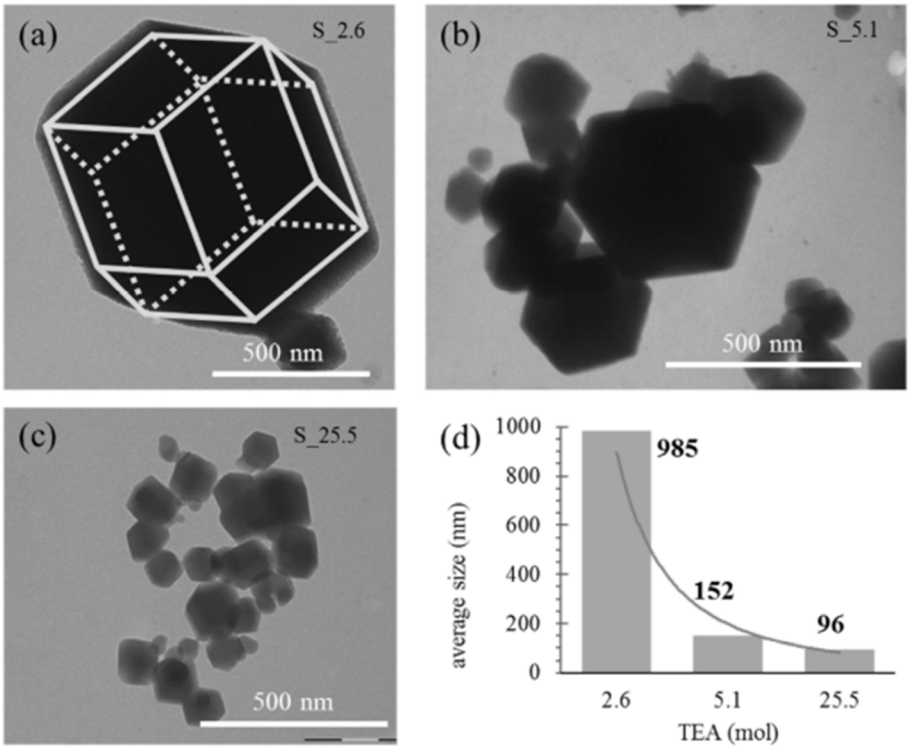

Fig. 7 The shape and size of ZIF-8 crystals synthesized upon addition of triethylamine at various equivalent Zn^{2+} ratios: (a) 2.6 mol; (b) 5.1 mol; (c) 25.5 mol. (d) Average particle size of ZIF-8. This figure has been reproduced from ref. 28 with permission from Elsevier, copyright 2017.

100 nm. A surfactant added into a 2-HMim solution in H_2O resulted in good dispersion of the obtained ZIF-8 particles.

Addition of additives influences the particle size of ZIF-8 crystals. For example, Butova *et al.*[28] found that increasing triethylamine (TEA) at various equivalent Zn^{2+} ratios of 2.6–25.5 mol resulted in decreased average particle size of ZIF-8 from 985 nm to 96 nm (Fig. 7). The authors critically rationalized the role of TEA as a structure-directing agent so that 2-HMim can interact with the Zn^{2+} ions favorably. As a result, the addition of TEA was minimized at 25.5 mol equivalent Zn^{2+} but still allowed the formation of small-size ZIF-8 particles.

By using machine learning analysis to assess the influence of synthetic variables, Allegretto *et al.*[72] predicted that the 2-HMim precursor concentration rather than the Zn^{2+} concentration was the most significant factor for synthesis of ZIF-8 in H_2O. A higher concentration of 2-HMim precursor led to a significant decrease in ZIF-8 crystallite size during the water-based syntheses.[29,31] Similarly, Nalesso *et al.*[42] used the ultrasound-assisted method for synthesis of ZIF-8 in H_2O at a high ratio of 2-HMim/Zn^{2+} (70 : 1) to obtain a small size of ZIF-8 nanocrystals (80 nm) using H_2O. However, the hydrothermal method appeared not to reduce the size of ZIF-8 despite the high 2-HMim/Zn^{2+} ratio of 57 : 1.[38] This phenomenon might be due to the high reaction temperature accelerating the nucleation and growth of ZIF-8 crystals that increase their size.

3.5. Morphology

ZIF-8 exhibits a wide range of morphologies such as hexagon, cube, rhombic dodecahedron, microsphere, and polyhedron, as shown in Table S1.† It is also found that polyhedra including dodecahedron and hexagon are common shapes of ZIF-8. The cubic shape of ZIF-8 has been rarely reported in previous studies.[44,73,74] It seems that there is no relationship between the ZIF-8 shape and synthesis method. However, conventional methods such as solvothermal and hydrothermal methods often result in the formation of dodecahedral or polyhedral shape. Meanwhile, the diversity of ZIF-8 shape appears to be more common in advanced synthesis methods such as US- and MW-assisted methods.

According to Table S1,† the solvent considerably affects the morphology of ZIF-8. As methanol is used as a solvent, ZIF-8 has two major shapes including polyhedron and dodecahedron. By contrast, in the solvothermal method, DMF was often used to synthesize ZIF-8 with diverse morphologies such as polyhedron, cube, hexagon, dodecahedron, and dodecahedron. Moreover, additives such as HCOONa and trimethylamine (TEA) or surfactants such as Pluronic P-123 commonly gave rise to the formation of ZIF-8 with a dodecahedral shape. Thus, the type of solvent and additives should be investigated to control the morphology of ZIF-8.

Speaking of the effect of synthesis methods, Lee *et al.*[75] conducted a range of synthesis methods (solvothermal using DMF and methanol, microwave-assisted, sono-chemical, mechanochemical, dry-gel conversion, and microfluidic) for morphological properties of ZIF-8 (Fig. S1†). The authors observed that all ZIF-8 crystals synthesized by the above methods exhibited a hexagonal morphology, which was different from the morphology of the commercial one. They

© 2025 The Author(s). Published by the Royal Society of Chemistry

Open Access Article. Published on 27 Mei 2025. Downloaded on 02/06/2026 13:51:38.
This article is licensed under a Creative Commons Attribution-NonCommercial 3.0 Unported Licence.

explained that the friction forces applied during the synthesis resulted in this difference. Therefore, synthesis methods may insignificantly affect the morphology of ZIF-8.

4. Biomedical applications of ZIF-8-based materials

4.1. Antibacterial properties

ZIF-8 has garnered significant attention in recent decades due to its exceptional properties with large pore sizes and versatile functions for the biomedical field. Notably, ZIF-8 serves as an antimicrobial agent capable of effectively eliminating bacteria. The antimicrobial action of ZIF-8 relies on releasing metal ions from the ZIF-8 structure or dopants to directly damage bacterial cell walls. This process leads to the production of reactive oxygen species (ROS), disruption of internal organelles, and degradation of glutathione (GSH).

Several studies investigated the effectiveness of ZIF-8-based materials for antibacterial applications. For example, Ahmad *et al.*[76] reported the development of ZIF-8 modified with functionalized graphene oxide (GO) containing amine groups through direct post-modification using an ammonium hydroxide solution. This ZIF-8/GO material was incorporated into a polyethersulfone (PES) matrix to form a composite film that exhibited significant antibacterial activity. The composite achieved antibacterial rates of 81.1% against *Escherichia coli* and 85.7% against *Staphylococcus aureus*.

Pei *et al.*[77] synthesized ZIF-8 using a conventional method, followed by heat treatment in an oxygen environment to produce thermally sensitive ZIF-8 (T-ZIF-8) for antibacterial applications. The results were remarkable with a bactericidal efficiency of 99.99% against *E. coli* and *S. aureus* within just 20 minutes. This result significantly surpassed the performance of the ZIF-8/GO composite reported by Ahmad *et al.*[76] The superior antibacterial activity was attributed to the photocatalytic properties of T-ZIF-8, which enhanced the generation of reactive oxygen species (ROS) such as $O_2^{\bullet-}$ and $OH^{\bullet}$. These radicals enabled more rapid bacterial destruction.

In another study, Zhang *et al.*[78] developed Cu(II)@ZIF-8, which Cu^{2+} ions were embedded within the porous structure of ZIF-8 to create a highly effective antibacterial agent. The results revealed that Cu(II)@ZIF-8 generated 3–4 times more reactive oxygen species (ROS) than ZIF-8 alone. This enhanced ROS production brought a strong antibacterial performance with a minimum inhibitory concentration (MIC) of 64 μg mL^{-1} against *S. aureus*. Thus, Cu(II)@ZIF-8 can be used as an antibacterial agent for biomedical applications such as wound healing.

Interestingly, Yang *et al.*[79] designed an antibacterial cotton-based ZIF-8 material, namely ZIF-8@PDMS fabric. This fabric displayed an outstanding antibacterial performance with 100% disinfection efficiency against *E. coli* and *S. aureus*. Additionally, the antibacterial efficiency of this composite remained high even after multiple durability tests, *i.e.*, 95% efficacy after five washing times and 98% efficacy after 300 times of rubbing cycles. Notably, ZIF-8-based nanocomposites showed promising therapeutic potential for accelerating the healing of infected wounds and leveraging their superior antibacterial and anti-inflammatory properties, as illustrated in Fig. 8. These results suggest that ZIF-8-based materials can be promising in practical applications.

4.2. Anticancer properties

As an emerging type of porous material, the zeolitic imidazolate framework (ZIF-8) offers several unique advantages, including high porosity, structural regularity with excellent modifiability, tunable surface functionalities, and notable anticancer activity. Several recent studies elucidated the anticancer mechanisms of ZIF-8.[81,82] Specifically, intrinsic metal ions (Zn^{2+}) or doped metal ions (Me^{n+}) can be released from ZIF-8-based composites to produce reactive oxygen species (ROS) for inducing cell death. Moreover, certain doped metal ions, such as Cu^{2+} and Fe^{2+}, can penetrate the cell interior and participate in Fenton reactions, which enable the generation of ROS such as $^{\bullet}OH$ to accelerate cellular destruction, as illustrated in Fig. 9.

The anticancer efficacy of ZIF-8-based materials has been well-documented. For example, Gao *et al.*[85] synthesized ZIF-8 using a self-template method, incorporated as-synthesized ZIF-8 with folic acid, Au, and CuS to form nanosized ZIF-8/Au/CuS/folic acid for anticancer applications. In this route, CuS enhanced chemodynamic therapy (CDT) by the generation of Cu(I), which catalytically decomposed H_2O_2 into hydroxyl radicals ($^{\bullet}OH$). These radicals effectively exterminated cancer cells (HepG2). The study reported that the cell viability of HepG2 was reduced to approximately 25%.

Hu *et al.*[83] fabricated a supramolecular O_2–Cu/ZIF-8@ZIF-8@WP6-methylene blue photosensitive system in combination with photodynamic therapy (PDT) against HepG2 cancer cells. The authors achieved remarkable results with only 5% of HepG2 cells surviving after treatment. This outcome revealed superior HepG2 anticancer efficacy of O_2–Cu/ZIF-8@ZIF-8@WP6-methylene blue compared to O_2–Cu/ZIF@Ce6/ZIF-8@F127, as reported by Gao *et al.*[85] As a result, the integration of ZIF-8 with WP6-methylene blue and PDT significantly enhances the synergistic effect in cancer therapy.

Recently, ZIF-8 has been widely doped with photosensitive components in photodynamic therapy (PDT), which promotes the generation of singlet oxygen ($^1O_2$) a highly toxic species that targets tumor cells upon irradiation.[86] This approach has proven to be highly effective in cancer treatment using ZIF-8-based materials.[83,84] The primary mechanism of action is suggested based on the production of singlet oxygen, which causes localized vascular stasis and leads to vascular hemorrhage and eventual destruction of the tumor walls.[87]

In another study, Li *et al.*[88] developed lanthanide-doped nanoparticles (LaNPs) coated with Fe/Mn bimetal-doped ZIF-8 for synergistic photodynamics/chemodynamics against HeLa cancer cells. The dual doping of Fe^{2+}/Mn^{2+} significantly reduced the band gap of the ZIF-8-based photosensitizer from 5.1 to 1.7 eV and facilitated the excitation of LaNPs/Fe/Mn-doped ZIF-8 nanocomposite. As a result, the anticancer effect was highly

Open Access Article. Published on 27 Mei 2025. Downloaded on 02/06/2026 13:51:38.
This article is licensed under a Creative Commons Attribution-NonCommercial 3.0 Unported Licence.

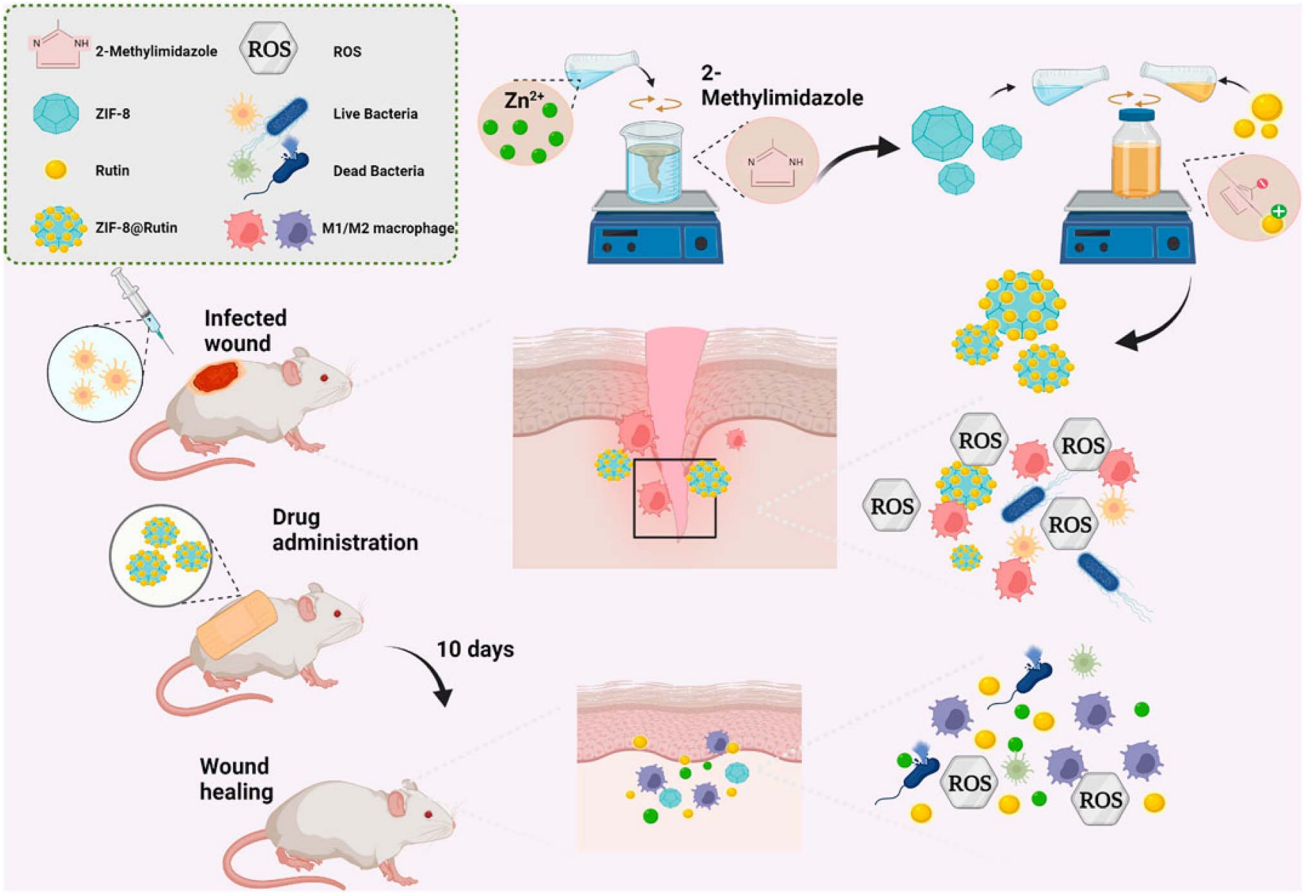

Fig. 8 Synergistic effect of the ZIF-8@rutin nanocomposite on eliminating bacteria and inflammatory response. Reactive oxygen species (ROS) and Zn^{2+} were released to destroy bacterial cells. Rutin could neutralize excessive ROS to mitigate wound inflammation and protect cells from oxidative stress. This dual functionality positions ZIF-8@rutin as a promising material for antibacterial, anti-inflammatory, and cell-protective applications. This figure has been reproduced from ref. 80 with permission from Frontiers Media SA, copyright 2022.

effective at 5% glutathione (GSH) remaining in the cancer cells. These recent advancements suggest that the combination of ZIF-8 materials with photodynamic and chemodynamic therapies holds great potential for future biomedical applications in cancer treatment.

4.3. Biosensing platform

The development of ultra-sensitive and highly selective biosensors is of significance for early disease diagnosis and monitoring treatment outcomes. Recently, ZIF-8-based biosensors have been designed to detect various targets, including biomarkers, microRNAs, and live cancer cells.[89,90] By tailoring and modifying the pore structure of ZIF-8, these composites provide an effective platform for the immobilization of enzymes and other substances in electrochemical sensors. Electrode surfaces modified with ZIF-8 materials enable two primary detection pathways, *e.g.*, antibody immobilization and aptamer immobilization. These strategies facilitate specific and sensitive detection of disease-related targets for the early diagnosis and timely treatment of various diseases.[91]

Several studies have highlighted the biosensing applications of ZIF-8-based materials. For instance, Meng *et al.*[92] reported a multifunctional ZIF-8-based biosensor incorporating graphene quantum dots for detecting M.SssI methyltransferases. These enzymes play a crucial role in catalyzing aberrant DNA methylation, which is associated with various diseases. Early detection of M.SssI methyltransferase activity could significantly contribute to therapeutic interventions. In this work, the ZIF-8-based biosensor exhibited a broad linear response range from 0.005 to 150 U mL^{-1} and achieved an impressive detection limit of 0.004 U mL^{-1}. Thus, ZIF-8-based biosensors can be useful for highly sensitive and specific biosensing therapies.

In another study, Roy *et al.*[93] designed a biosensor system based on the enzyme ZIF-8/acetylcholinesterase for the early diagnosis of Hirschsprung's disease (Fig. 10a). Hirschsprung's disease is a congenital condition characterized by the absence of nerve cells at the end of the intestine in infants and young children. Normally, the gut contains numerous nerve cells along its length that regulate the intestinal function. Without these nerve cells, the intestines lose functionality, leading to blockages, infections, and potentially fatal outcomes.[95] The ZIF-

© 2025 The Author(s). Published by the Royal Society of Chemistry

Open Access Article. Published on 27 Mei 2025. Downloaded on 02/06/2026 13:51:38.
This article is licensed under a Creative Commons Attribution-NonCommercial 3.0 Unported Licence.

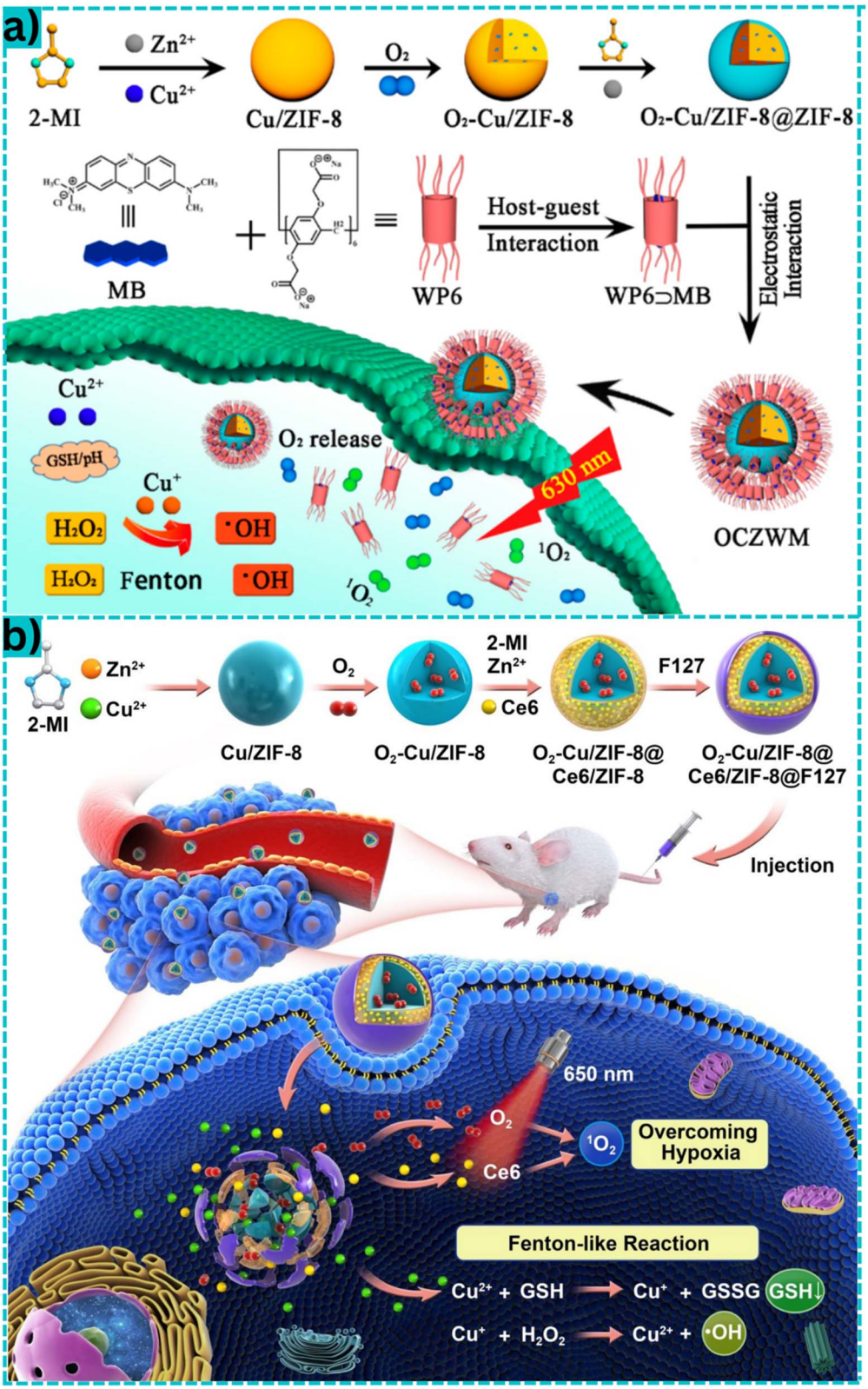

Fig. 9 (a) The schematic synthesis of O_2–Cu/ZIF-8@ZIF-8@WP6-methylene blue materials for HepG2 anti-cancer photodynamic therapy (PDT). The combination of PDT and Cu^{2+} therapy in the material produces a series of effects on cancer cells: (1) increasing the concentration of singlet oxygen ($^1O_2$) in the tumor microenvironment and (2) decreasing the concentration of glutathione (GSH) by reacting with GSH to form Cu^+, which then participates in the Fenton-like reactions. Abbreviations: WP6-MB, WP6-methylene blue; OCZWN, O_2–Cu/ZIF-8@ZIF-8@WP6-methylene blue; GSH, glutathione. This figure has been reproduced from ref. 83 with permission from MDPI, copyright 2021. (b) The synthesis process of O_2–Cu/ZIF@Ce6/ZIF-8@F127 materials and their cancer cell-killing mechanism. Specifically, chlorin e6 (Ce6), upon laser irradiation, enhances the efficacy of photodynamic therapy (PDT). Cu^{2+} is released to consume intracellular GSH and initiate a Fenton-type reaction, enabling chemodynamic therapy (CDT). This figure has been reproduced from ref. 84 with permission from American Chemical Society, copyright 2019.

© 2025 The Author(s). Published by the Royal Society of Chemistry

Open Access Article. Published on 27 Mei 2025. Downloaded on 02/06/2026 13:51:38.
This article is licensed under a Creative Commons Attribution-NonCommercial 3.0 Unported Licence.

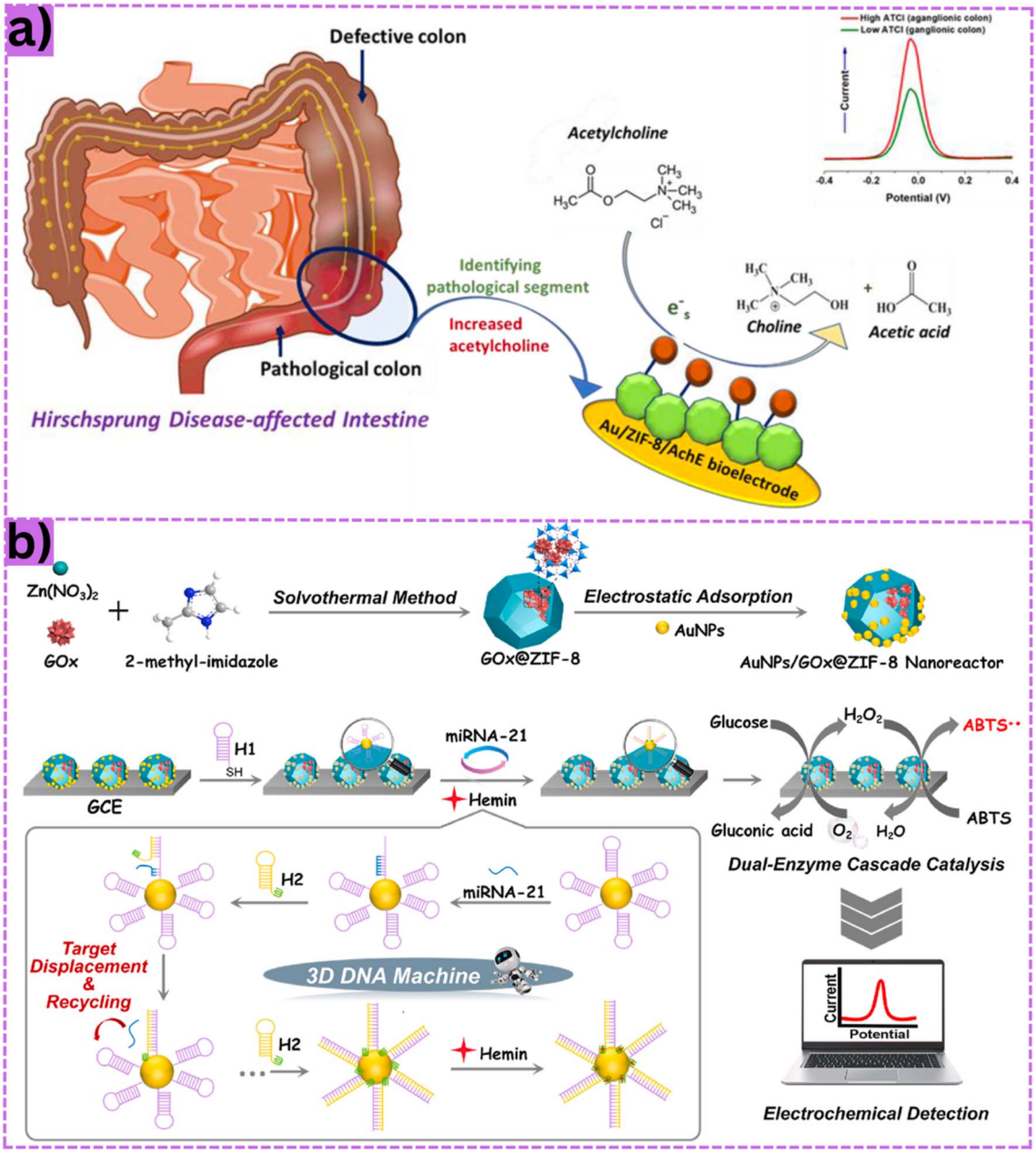

Fig. 10 (a) Early diagnosis of Hirschsprung's disease using the Au/ZIF-8/AchE system, in which ZIF-8 was incorporated with the enzyme acetylcholinesterase (AchE) and Au. This system detected Hirschsprung's disease through acetylcholine as a primary biomarker. This figure has been reproduced from ref. 93 with permission from John Wiley and Sons, copyright 2022. (b) The formation of an electrochemical biosensor, namely AuNPs/GOx@ZIF-8. This sensor facilitated a target miRNA-activated 3D DNA walker and enabled cascade catalysis for amplified miRNA detection. Abbreviations: GCE, glassy carbon electrode; ABTS, 2,2′-azino-bis(3-ethylbenzothiazoline-6-sulfonic acid); Gox, glucose oxidase; NPs, nanoparticles. This figure has been reproduced from ref. 94 with permission from Elsevier, copyright 2022.

8/acetylcholinesterase biosensor exhibited high sensitivity for early diagnosis with a detection limit (LOD) of 0.19 μM.

Similarly, Kong *et al.*[94] developed an electrochemical sensor using Gox-doped ZIF-8 nanoreactors and Au nanoparticles combined with a 3D DNA walker for sensitive and selective detection of microRNA (miRNA), as described in Fig. 10b. This system successfully detected miRNA-21 in HeLa and MCF-7 cancer cells and achieved an impressively low detection limit of 2.9×10^{-5} μM. In another study, Zhang *et al.*[96] fabricated a new ZIF-8-based electrochemical aptasensor for the detection of human epidermal growth factor receptor-2 (HER2) and estrogen receptor (ER) biomarkers. This electrochemical aptasensor had exceptional sensitivity with detection limits of 3.8 fg mL^{-1} for HER2 and 6.8 fg mL^{-1} for the ER within just 60 minutes. These findings underscore the significant potential of ZIF-8-based materials in the early and precise diagnosis of specific diseases such as cancer.

© 2025 The Author(s). Published by the Royal Society of Chemistry

Open Access Article. Published on 27 Mei 2025. Downloaded on 02/06/2026 13:51:38.
This article is licensed under a Creative Commons Attribution-NonCommercial 3.0 Unported Licence.

4.4. Bioimaging

The advancement of diagnostic materials in medicine has led to the exploration of innovative modalities for cancer treatment. Among these, ZIF-8-based nanoplatforms are used in magnetic resonance imaging (MRI), computed tomography (CT), and photoacoustic imaging (PAI), as outlined in Table S2.† Indeed, ZIF-8-based materials can be tailored for dual- or tri-modal imaging to enhance diagnostic precision. For MRI applications, imaging activity is evaluated based on the longitudinal (T_1) and transverse (T_2) relaxation rates of water protons. The reciprocals of these values, denoted as recovery rates R_1 and R_2, serve as the longitudinal and transverse recovery coefficients, respectively.[97] With a sufficient relaxivity ratio ($\alpha = R_2/R_1$), ZIF-8-based materials are applied in advanced cancer diagnostics through highly accurate and multi-functional imaging techniques (Fig. 11a).

Guo *et al.*[99] designed a multifunctional ZIF-8-based nanoplatform, surface-coated by a polydopamine (PDA) shell, modified with Mn^{2+} and polyethylene glycol, and incorporated doxorubicin (DOX) as a therapeutic agent. The PDA shell acted as an effective enhancer for photothermal therapy (PTT) and photoacoustic imaging (PAI) because this coating possessed a good photothermal conversion rate, while Mn^{2+} functioned as

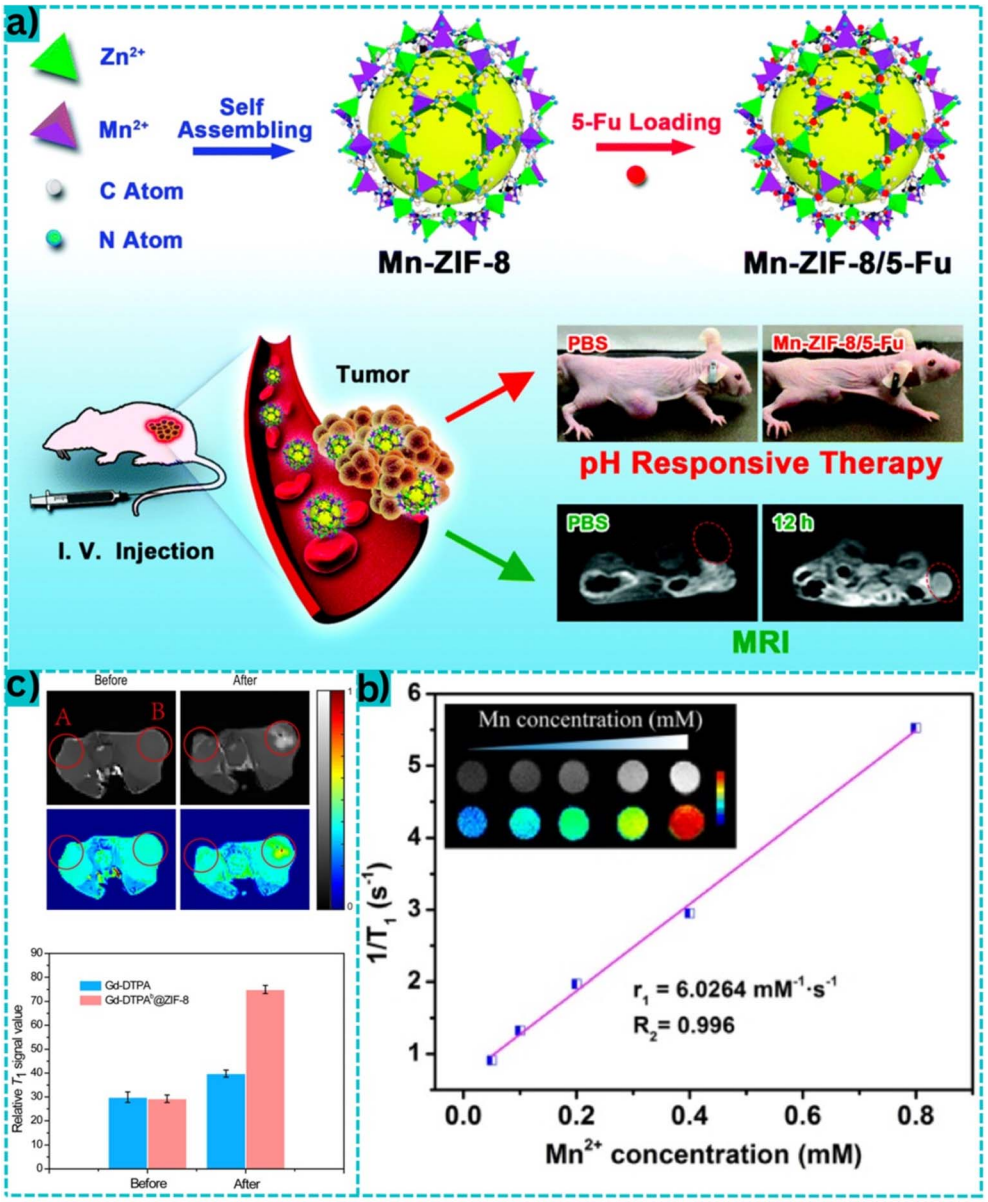

Fig. 11 (a) The assembling process of ZIF-8 incorporating Mn^{2+} as a contrast agent for magnetic resonance imaging (MRI) applications. Loading the anticancer drug 5-fluorouracil (5-Fu) enables Mn-ZIF-8/5-Fu to exhibit pH responsive cancer treatment and imaging. This figure has been reproduced from ref. 98 with permission from Royal Society of Chemistry, copyright 2019. (b) T_1 relaxation rates (R_1) and *in vitro* T_1-weighted MR images of ZIF-8/DMPP at different concentrations. This figure has been reproduced from ref. 99 with permission from Dove Medical Press, copyright 2020. (c) MR images before and after Gd-DTPA@ZIF-8 injection in mice. T_1 MRI signal values before and after Gd-DTPA (side A) and Gd-DTPA@ZIF-8 (side B) injections. This figure has been reproduced from ref. 100 with permission from Springer, copyright 2021.

Open Access Article. Published on 27 Mei 2025. Downloaded on 02/06/2026 13:51:38.
This article is licensed under a Creative Commons Attribution-NonCommercial 3.0 Unported Licence.

a contrast agent for magnetic resonance imaging (MRI). The authors observed a significant improvement in both *in vivo* MRI and PAI of tumor-bearing mice compared to controls without the nanoplatform. Notably, the study achieved an R_1 value of 6.03 mM^{-1} s^{-1} (Fig. 11b). This outcome confirms the great potential of ZIF-8-based nanoplatforms for integrated diagnostic and therapeutic applications.

Following the same trend, Zhou *et al.*[100] developed an advanced T_1 MRI contrast agent by loading Gd-chelate (Gd-DTPA) onto a ZIF-8 framework, as shown in Fig. 11c. The resulting material achieved an R_1 value of 29.60 mM^{-1} s^{-1}, significantly surpassing the performance reported by Guo *et al.*[99] This value was so far higher than that of single Gd-DTPA. As a result, Gd-DTPA/ZIF-8 enhanced MRI contrast compared to conventional materials. Recently, Pandit *et al.*[101] integrated dual MOF (ZIF-8/ZIF-67) with iron oxide (IO) nano and decorated with folic acid (FA) as the targeting agent to produce a novel Fe_3O_4@ZIF-8@ZIF-67@FA nanocomposite. The inclusion of superparamagnetic iron nanoparticles significantly improved the magnetic resonance imaging (MRI) performance of this nanocomposite and achieved an impressive R_2 value of 85.86 mM^{-1} s^{-1}. In addition to bioimaging, this nanoplatform also exhibited selective anticancer properties due to FA coating on the surface. Cancer cells overexpress folic acid receptors, and hence FA-conjugated systems are effective in targeting these cells. This selective targeting ability of ZIF-8-based materials gives the therapeutic potential in delivering anticancer drugs precisely to folic acid-overexpressing cells. To sum up, the multifunctionality of ZIF-8 materials, combining therapeutic and diagnostic features, underlines their promise for integrated cancer treatment and imaging. These findings pave the way for further innovation of ZIF-8-based bioimaging agents in tumor diagnosis and therapy.

4.5. Drug delivery system

ZIF-8-based nanomaterials are distinguished by their inherent porous structure, high drug-loading capacity, pH-sensitive drug release, and remarkable thermal and chemical stability. These attributes make ZIF-8-based nanomaterials an exceptional candidate for advanced drug delivery systems.[100] The use of pH stimuli for targeted drug delivery, particularly in cancer therapy has been well documented.[102] This is primarily attributed to the acidic microenvironment characteristic of tumor sites. Additionally, pH-responsive properties of ZIF-8 are advantageous in oral drug delivery systems, enabling drugs to bypass the acidic gastric environment and be efficiently absorbed in the alkaline conditions of the small intestine. Table S2† provides an overview of ZIF-8-based materials as potential nanostructured systems for intelligent and controlled drug release.

Several studies investigated the adaptability of ZIF-8 in pH-responsive drug delivery systems. For example, Lei *et al.*[103] synthesized a ZIF-8-based pH-responsive nanocomposite grown on the surface of the poly(ε-caprolactone)-*block*-poly(-quaternized vinylbenzyl chloride/bipyridine) polymers. Then, the drug doxorubicin hydrochloride (DOX) was loaded into the cores of the micelles or internal cavities, while ZIF-8 functioned as a protective agent to release the targeted drug. Accordingly, the results showed that 80% DOX was released at pH 5.5 compared to only 10% at pH 7.4.

Following the same trend, Yan *et al.*[104] anchored a *cis*-aconitic anhydride-doxorubicin (CAD) prodrug within ZIF-8 and coated with folic acid (FA) for enhanced cancer-targeting efficacy. This system achieved a highly controlled release in three stages: (i) FA dissociation at acidic pH, (ii) ZIF-8 structural disruption, and (iii) cleavage of the pH-sensitive linker. As a result, drug control in normal cells and drug release efficiency in cancer cells were both enhanced. Remarkably, more than 95% of DOX was released at pH 5.5, and a negligible release rate was observed at pH 7.4. Thus, this novel pre-drug-ZIF-8 strategy opened a new pathway in drug delivery to the target.

In addition to cancer-targeting mechanisms, ZIF-8-based materials has been employed to improve the bioavailability of oral drugs by protecting them from stomach acidity and facilitating their release in the small intestine. For instance, Zhu *et al.*[105] combined the succinylated-zein drug carrier with ZIF-8 to create an effective pharmaceutical carrier (Fig. 12a). When loaded with indomethacin, a non-steroidal anti-inflammatory drug, the system released 17% indomethacin drug into the simulated gastric fluid over 2 h, and complete release into the simulated intestinal fluid was achieved within 6 h. As a result, this system might have high efficiency for oral drug delivery.

Considering the usual blood and oral pH-responsive drug delivery routes, Yin *et al.*[107] have developed a smart drug delivery system that responds to ambient glucose levels in the treatment of diabetes. In this study, ZIF-8 was synthesized by co-precipitation and encapsulated with glucose oxidase (GOx), Au nanoparticles and metformin a diabetes drug. The main principle of this drug delivery system is that GOx can react with glucose to produce gluconic acid and H_2O_2. Meanwhile, Au nanoparticles catalyze H_2O_2 decomposition to produce O_2, forming a self-sustaining cycle. This responsive material collapsed at high glucose concentrations, releasing over 80% of metformin within 24 h. This drug delivery system also holds promise for diabetes treatment in hypoxic environments.

Mi *et al.*[106] created a ZIF-8-based folate receptor-mediated response drug delivery system, which was designed for tumor-targeted drug delivery. This system exhibited high baicalin-loading efficiency and released significant quantities of baicalin in the acidic microenvironment of cancer tumors (Fig. 12b). To sum up, these studies indicated the multifunctionality and versatility of ZIF-8-based materials in pH-responsive and glucose-responsive systems for drug delivery applications. They are also expected to apply in the biomedical field such as targeted therapy, oral drug delivery, and smart drug release technologies.

4.6. Bone tissue engineering

The bone tissue has a natural capacity to heal minor injuries, such as small cracks or certain types of fractures. However, severe conditions, including trauma, infections, tumors, or large critical-size defects, often exceed this self-healing threshold and require external intervention.[108] Bone tissue

© 2025 The Author(s). Published by the Royal Society of Chemistry

Open Access Article. Published on 27 Mei 2025. Downloaded on 02/06/2026 13:51:38.
This article is licensed under a Creative Commons Attribution-NonCommercial 3.0 Unported Licence.

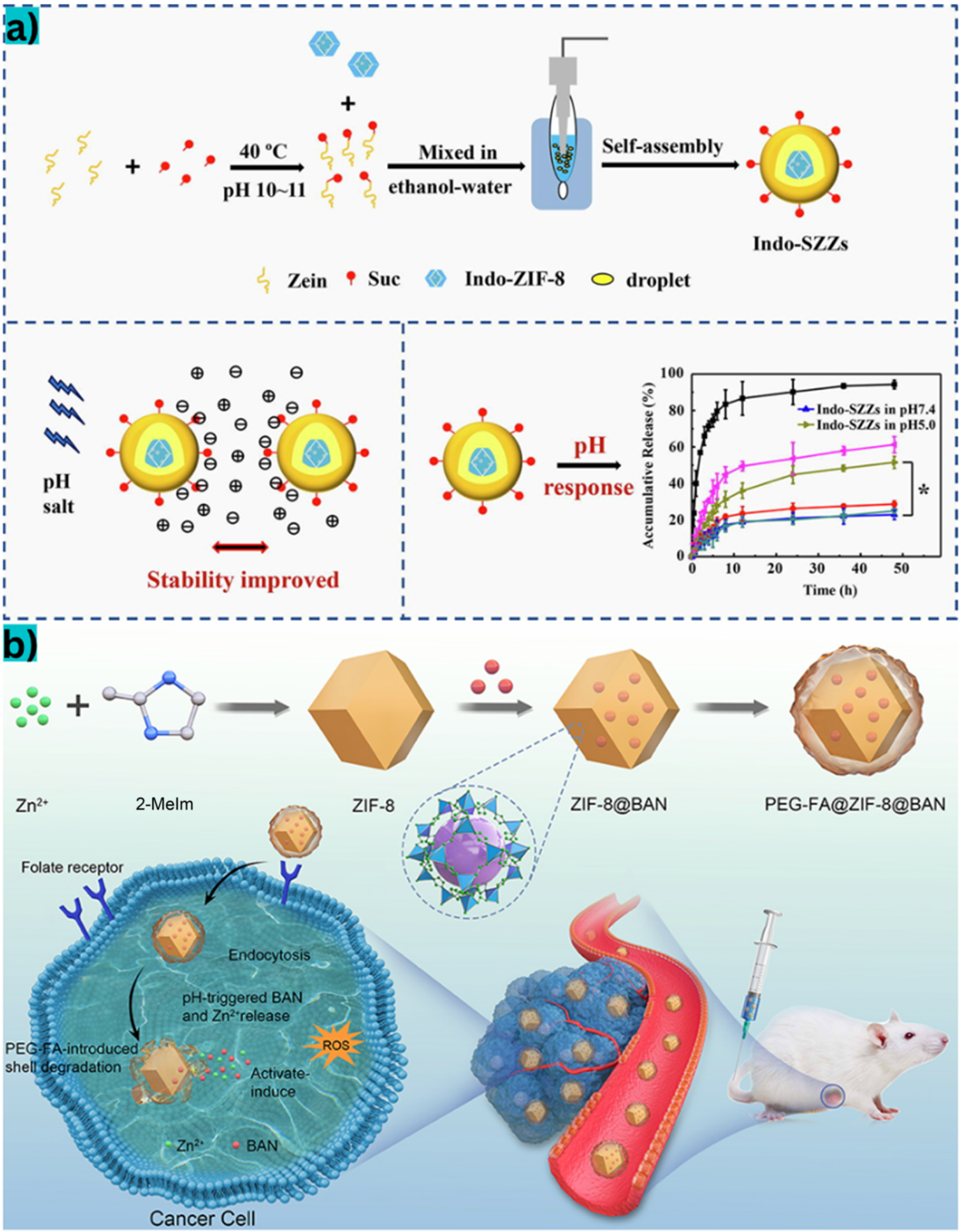

Fig. 12 (a) An orally pH-responsive indomethacin drug delivery system synthesized by combining succinylated zein with ZIF-8. This system showed a controlled drug release profile in simulated gastric and intestinal environments. Abbreviations: Indo-SZZs, indomethacin-succinylated-zein/ZIF-8. This figure has been reproduced from ref. 105 with permission from Elsevier, copyright 2020. (b) The synthesis of a ZIF-8-based folate receptor-mediated response drug delivery system. This system was designed for tumor-targeted drug delivery and exhibited high drug-loading efficiency and stable drug release in the acidic microenvironment of tumors. Abbreviations: BAN, baicalin; PEG-FA, polyethylene glycol-folate. This figure has been reproduced from ref. 106 with permission from Dove Medical Press, copyright 2021.

© 2025 The Author(s). Published by the Royal Society of Chemistry

Open Access Article. Published on 27 Mei 2025. Downloaded on 02/06/2026 13:51:38.
This article is licensed under a Creative Commons Attribution-NonCommercial 3.0 Unported Licence.

engineering offers solutions for the repair and regeneration of bone tissue. Thanks to the porous structure and drug-loading capability, ZIF-8 has emerged as a promising material in this field. Incorporating nano-ZIF-8 crystals into polymer scaffolds at safe concentrations is expected to improve the mechanical properties and enhances scaffold stability. This nano-ZIF-8/polymer scaffolds can be a versatile candidate for bone tissue engineering applications.[109]

Many studies have explored that ZIF-8-nano-based titanium implants can promote bone integration, osteogenesis, angiogenesis, and healing of major bone defects, as shown in Table S2.† Bone tissue has slower blood flow compared to other organs. This limits the effectiveness of conventional systemic treatments because drugs are partly/completely metabolized or excreted or accumulated in tissues/organs before they reach the bone.[15] By encapsulating therapeutic agents within ZIF-8 and adding them into scaffolds, targeted delivery is achieved to promote tissue regeneration and faster healing of major bone defects.

Alkaline phosphatase (ALP) assays are commonly used to evaluate osteogenic differentiation in bone regeneration studies, as ALP is an early marker of cellular mineralization. Enhanced ALP activity indicates effective support for bone tissue regeneration.[110] For example, Tao *et al.*[111] fabricated ZIF-8 nanoparticles loaded with levofloxacin (Levo) and deposited them on collagen-modified Ti substrates by cathode electrophoresis deposition. Then, multilayers of gelatin (Gel) and chitosan (Chi) were spin-coated onto the modified Ti substrate surface. This system showed good ALP activity at approximately 2.2 μg *p*-nitrophenol per mg protein and enhanced collagen secretion.

Hyperlipidemia, which adversely affects bone formation and healing, can also be addressed using ZIF-8-based systems. Qiao

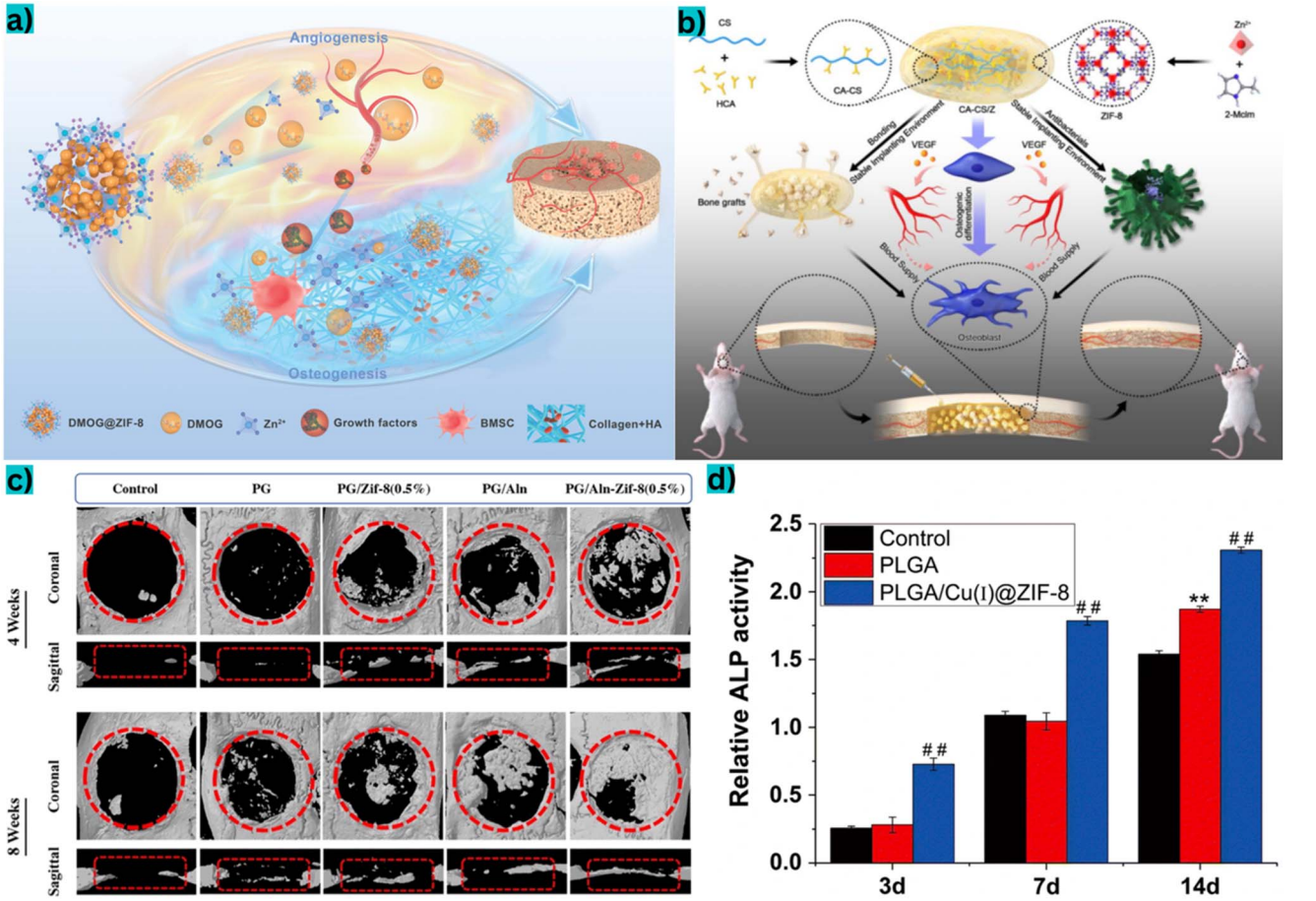

Fig. 13 (a) A dimethyloxallyl glycine-loaded ZIF-8 framework system for enhancing bone angiogenesis. Abbreviation: DMOG@ZIF-8, dimethyloxallyl glycine-loaded ZIF-8. This figure has been reproduced from ref. 114 with permission from John Wiley and Sons, copyright 2022. (b) A multifunctional bone adhesion hydrogel derived from catechol-chitosan (CA-CS/Z) with ZIF-8. This material acts as an antibacterial, biologically functional adhesive that facilitates bone formation, stabilizes the implant environment, and supports vascularization. Abbreviations: CA-CS/Z, catechol-chitosan multifunctional hydrogels; VEGF, vascular endothelial growth factor. This figure has been reproduced from ref. 115 with permission from American Chemical Society, copyright 2022. (c) CT images comparing bone regeneration in mouse skull defects treated with ZIF-8-based materials and control samples at 4 and 8 weeks. Red dotted lines mark the initial boundaries of critical cranial defects, which showed improved healing with PG/Aln-ZIF-8. Abbreviations: PG, polycaprolactone/gelatin; PG/Aln-ZIF-8, PG with alendronate-loaded ZIF-8. This figure has been reproduced from ref. 113 with permission from Elsevier, copyright 2022. (d) Comparative ALP activity indicates the osteogenic difference between ZIF-8-based materials and control samples. Abbreviations: PLGA, polycaprolactone/gelatin; ALP, alkaline phosphatase. This figure has been reproduced from ref. 116 with permission from Springer Nature, copyright 2020.

© 2025 The Author(s). Published by the Royal Society of Chemistry

Open Access Article. Published on 27 Mei 2025. Downloaded on 02/06/2026 13:51:38. This article is licensed under a Creative Commons Attribution-NonCommercial 3.0 Unported Licence.

et al.[112] developed a simvastatin-laden ZIF-8 biohydrogel modified with poly(ethylene glycol) diacrylate (PEGDA) and sodium alginate (SA), denoted as SIM@ZIF-8/PEGDA/SA. This biohydrogel stimulated osteogenic differentiation while inhibiting adipocyte formation and achieved a relative ALP activity (OD value/total protein) of 3. To improve ALP values, Al-Baadani *et al.*[113] designed polycaprolactone/gelatin (PG) membranes embedded with alendronate-loaded ZIF-8. *In vitro* studies using MC3T3-E1 and RAW264.7 cells showed enhanced anti-osteoporotic properties, with a relative ALP activity of 5 and collagen secretion of 0.8. In addition, this ZIF-8-based material exhibited excellent antibacterial activity by disinfecting 94% *E. coli* and *S. aureus* bacteria.

The innovative ZIF-8-based biomaterials hold great potential to address multiple challenges in bone tissue engineering (Fig. 13). They can accelerate early osteoblastogenesis, combat hyperlipidemia, and provide effective antibacterial action; hence, they are promising materials for osteoporosis treatment and infection control. Despite these advancements, concerns regarding the biocompatibility and long-term toxicity of ZIF-8 still remain. Further studies should evaluate the safety of ZIF-8 in bone tissue engineering and possible effects on the human body.

5. Limitations and future prospects

5.1. Limitations

Although ZIF-8-based materials exhibited biomedical potentials, several limitations need to be addressed. Firstly, the leaching of ZIF-8 or degradation into Zn^{2+} ions should be investigated because this process could cause cytotoxicity at high concentrations. For example, Yang *et al.*[117] indicated that both ZIF-8 exhibited significant toxic effects on the benthic organism *Corbicula fluminea*, due to the accumulation of ZIF-8 and the release of Zn^{2+} inducing oxidative stress. Joo *et al.*[25] found ZIF-8 and its decomposition products such as 2-methylimidazole and Zn^{2+} delayed the breeding time up to 80% of the F1 *Artemia*. Moreover, 2-methylimidazole exhibited high reproductive toxicity to F0 and F1 *Artemia*. It is also suggested that long-term *in vivo* studies are necessary to understand possible risks of chronic exposure and ensure the safety for clinical use. Secondly, as mentioned above, ZIF-8 can be synthesized using various methods, but there may still remain challenges to replicate it on a large scale. Maintaining specific properties of ZIF-8, *e.g.*, pore size, functional groups, or hybrid compositions can be another challenge. As a result, developing cost-effective, scalable, and reproducible synthesis methods is essential for commercial and clinical viability. Thirdly, it was shown that pH-sensitive drug release of ZIF-8-based materials is advantageous in some contexts, such as targeting acidic tumor environments, but it could be a drawback in neutral or slightly basic physiological conditions. Moreover, controlling the drug release rate without compromising other material properties remains a challenge. Finally, many concerns about the long-term interaction of ZIF-8 materials with the immune system and their clearance mechanisms from the body are not fully understood. These materials that remain in the body for extended periods could trigger inflammatory responses or accumulate in organs, causing unintended side effects.

5.2. Future prospects

As mentioned above, eco-friendly and cost-effective synthesis methods using water and inexpensive precursors may be a perspective to produce ZIF-8-based materials. More efforts to minimize the release of by-products such as toxic solvents, 2-methylimidazole and zinc, into the environment will become a key strategy in future studies. While conventional synthesis of ZIF-8-based materials should be considered, innovative methods can be an alternative solution. For example, the rapid and solvent-free or solvent-less mechanosynthesis of ZIF-8 can be a promising development.[59]

The versatility and unique properties of ZIF-8-based materials position them as promising candidates for various applications in biomedical engineering. Their inherent porosity, high surface area, tunable chemistry, biocompatibility, and pH-sensitive drug release offer significant advantages in drug delivery, imaging, and tissue engineering. By combining these advantages, ZIF-8 materials can integrate multifunctional systems. This integration opens new opportunities for simultaneously delivering therapeutic agents, monitoring treatment progress, and providing imaging for diagnostic precision.

As precision medicine gains traction, ZIF-8-based systems could play a vital role in creating personalized therapeutic platforms. For instance, encapsulating drugs in a controlled manner can be tailored to specific diseases or patient profiles. Emerging trends in artificial intelligence and machine learning could further optimize ZIF-8 formulations for patient-specific needs. Moreover, by incorporating bioactive molecules and growth factors, future ZIF-8-based materials could create bio-inspired scaffolds capable of mimicking natural tissue environments more effectively.

6. Conclusion

This review clarifies several synthesis strategies and structural characterization studies of ZIF-8 crystals. Remarkable attention is paid to innovative methods using green solvents such as water under the microwave or ultrasound assistance for tunable and sustainable synthesis of ZIF-8 with specific properties. ZIF-8-based materials represent potential applications in biomedical engineering fields such as antibacterial, anticancer, biosensing, bioimaging, and drug delivery. However, to translate ZIF-8-based materials into clinical trials, limitations such as toxicity, scalability, and regulatory compliance should be addressed. Future studies should prioritize understanding long-term biocompatibility, optimizing material properties for specific biomedical applications, and advancing scalable, eco-friendly synthesis techniques. Addressing these challenges could disclose new frontiers of ZIF-8-based materials, paving the way for innovative solutions in medicine.

Data availability

The data supporting this article have been included as part of the ESI.†

Open Access Article. Published on 27 Mei 2025. Downloaded on 02/06/2026 13:51:38. This article is licensed under a Creative Commons Attribution-NonCommercial 3.0 Unported Licence.

Conflicts of interest

The authors declare that they have no known competing financial interests or personal relationships that could have appeared to influence the work reported in this paper.

Acknowledgements

This work was funded by the Foundation for Science and Technology Development at Nguyen Tat Thanh University, Vietnam.

References

1 H. Wang, X. Pei, M. J. Kalmutzki, J. Yang and O. M. Yaghi, *Acc. Chem. Res.*, 2022, **55**, 707–721.
2 Z. Zheng, Z. Rong, H. L. Nguyen and O. M. Yaghi, *Inorg. Chem.*, 2023, **62**, 20861–20873.
3 K. S. Park, Z. Ni, A. P. Cote, J. Y. Choi, R. Huang, F. J. Uribe-Romo, H. K. Chae, M. O'Keeffe and O. M. Yaghi, *Proc. Natl. Acad. Sci. U. S. A.*, 2006, **103**, 10186–10191.
4 O. M. Linder-Patton, T. J. de Prinse, S. Furukawa, S. G. Bell, K. Sumida, C. J. Doonan and C. J. Sumby, *CrystEngComm*, 2018, **20**, 4926–4934.
5 Z. Sun, B. Sun, J. Xue, J. He, R. Zhao, Z. Chen, Z. Sun, H. K. Liu and S. X. Dou, *Adv. Funct. Mater.*, 2024, e2414671.
6 Y. Song, C. Yu, D. Ma and K. Liu, *Coord. Chem. Rev.*, 2024, **499**, 215492.
7 P. Nezhad-Mokhtari, R. Rahbarghazi, H. Hamishehkar, P. Asadi and M. Milani, *J. Polym. Environ.*, 2024, **32**, 6211–6234.
8 N. N. Sheno, S. Farhadi, A. Maleki and M. Hamidi, *New J. Chem.*, 2019, **43**, 1956–1963.
9 M.-W. Liu, G. Liu, Y.-F. Wang, B.-X. Lei and W.-Q. Wu, *Mater. Chem. Front.*, 2024, **8**, 869–879.
10 M. A. Nazir, S. Ullah, M. U. Shahid, I. Hossain, T. Najam, M. A. Ismail, A. Rehman, M. R. Karim and S. S. A. Shah, *Sep. Purif. Technol.*, 2025, **356**, 129828.
11 A. Maleki, M. Shahbazi, V. Alinezhad and H. A. Santos, *Adv. Healthc. Mater.*, 2020, **9**, 202000248.
12 Q. Wang, Y. Sun, S. Li, P. Zhang and Q. Yao, *RSC Adv.*, 2020, **10**, 37600–37620.
13 S. Feng, X. Zhang, D. Shi and Z. Wang, *Front. Chem. Sci. Eng.*, 2021, **15**, 221–237.
14 H. Tang, Y. Yu, X. Zhan, Y. Chai, Y. Zheng, Y. Liu, D. Xia and H. Lin, *J. Control. Release*, 2024, **365**, 558–582.
15 V. Hoseinpour and Z. Shariatinia, *Tissue Cell*, 2021, **72**, 101588.
16 M. Kermanian, S. Nadri, P. Mohammadi, S. Iravani, N. Ahmadi, V. Alinezhad, M.-A. Shokrgozar, M. Haddad, E. Mostafavi and A. Maleki, *J. Control. Release*, 2023, **359**, 326–346.
17 L. Bazzi, I. Ayouch, H. Tachallait and S. EL Hankari, *Results Eng.*, 2022, **13**, 100378.
18 S. Tanaka, K. Sakamoto, H. Inada, M. Kawata, G. Takasaki and K. Imawaka, *Langmuir*, 2018, **34**, 7028–7033.
19 Y. Wang, H. Zhang, X. Wang, C. Zou, B. Meng and X. Tan, *Ind. Eng. Chem. Res.*, 2019, **58**, 19511–19518.
20 P. Neelakanda, E. Barankova and K.-V. Peinemann, *Microporous Mesoporous Mater.*, 2016, **220**, 215–219.
21 M. Schelling, M. Kim, E. Otal, M. Aguirre and J. P. Hinestroza, *Cellulose*, 2020, **27**, 6399–6410.
22 H. Dai, X. Yuan, L. Jiang, H. Wang, J. Zhang, J. Zhang and T. Xiong, *Coord. Chem. Rev.*, 2021, **441**, 213985.
23 A. F. Gross, E. Sherman and J. J. Vajo, *Dalton Trans.*, 2012, **41**, 5458–5460.
24 K. Kida, M. Okita, K. Fujita, S. Tanaka and Y. Miyake, *CrystEngComm*, 2013, **15**, 1794.
25 H. S. Joo, S. A. Johari, M. B. Tayemeh, R. D. Handy, H. Abaei, N. Clark, J. Seyedi and M. A. Jones, *Environ. Pollut.*, 2024, **342**, 123141.
26 N. T. T. Nguyen, T. T. T. Nguyen, D. T. C. Nguyen and T. V. Tran, *Sci. Total Environ.*, 2024, **906**, 167295.
27 H. A. Kiwaan, F. Sh. Mohamed, N. A. El-Ghamaz, N. M. Beshry and A. A. El-Bindary, *J. Mol. Liq.*, 2021, **338**, 116670.
28 V. V. Butova, A. P. Budnyk, E. A. Bulanova, C. Lamberti and A. V. Soldatov, *Solid State Sci.*, 2017, **69**, 13–21.
29 L. Cheng, P. Yan, X. Yang, H. Zou, H. Yang and H. Liang, *Mater. Chem. Phys.*, 2020, **247**, 122869.
30 X. Xu, X. Zhang, Z. Xia, R. Sun, H. Li, J. Wang, S. Yu, S. Wang and G. Sun, *J. Energy Chem.*, 2021, **54**, 579–586.
31 A. Jamal Sisi, M. Fathinia, A. Khataee and Y. Orooji, *J. Mol. Liq.*, 2020, **308**, 113018.
32 Y. Wang, Y.-J. Hu, X. Hao, P. Peng, J.-Y. Shi, F. Peng and R.-C. Sun, *Adv. Compos. Hybrid Mater.*, 2020, **3**, 267–284.
33 D. Nunes, A. Pimentel, L. Santos, P. Barquinha, L. Pereira, E. Fortunato and R. Martins, in *Metal Oxide Nanostructures*, Elsevier, 2019, pp. 21–57.
34 K. Ahmad, H. U. R. Shah, M. Ashfaq, S. S. A. Shah, E. Hussain, H. A. Naseem, S. Parveen and A. Ayub, *Food Chem. Toxicol.*, 2021, **149**, 112008.
35 A. Nandagudi, S. H. Nagarajarao, M. S. Santosh, B. M. Basavaraja, S. J. Malode, R. J. Mascarenhas and N. P. Shetti, *Mater. Today Sustain.*, 2022, **19**, 100214.
36 H. Sonia, S. Kumari, S. Chahal, S. Devi, S. Kumar, S. Kumar, P. Kumar and A. Kumar, *Appl. Phys. A*, 2023, **129**, 91.
37 S.-H. Feng and G.-H. Li, in *Modern Inorganic Synthetic Chemistry*, Elsevier, 2017, pp. 73–104.
38 R. Li, W. Li, C. Jin, Q. He and Y. Wang, *J. Alloys Compd.*, 2020, **825**, 154008.
39 M. Malekmohammadi, S. Fatemi, M. Razavian and A. Nouralishahi, *Solid State Sci.*, 2019, **91**, 108–112.
40 C. Vaitsis, G. Sourkouni and C. Argirusis, *Ultrason. Sonochem.*, 2019, **52**, 106–119.
41 V. Safarifard and A. Morsali, *Coord. Chem. Rev.*, 2015, **292**, 1–14.
42 S. Nalesso, G. Varlet, M. J. Bussemaker, R. P. Sear, M. Hodnett, R. Monteagudo-Oliván, V. Sebastián, J. Coronas and J. Lee, *Ultrason. Sonochem.*, 2021, **76**, 105616.
43 H.-Y. Cho, J. Kim, S.-N. Kim and W.-S. Ahn, *Microporous Mesoporous Mater.*, 2013, **169**, 180–184.

© 2025 The Author(s). Published by the Royal Society of Chemistry

Open Access Article. Published on 27 Mei 2025. Downloaded on 02/06/2026 13:51:38.
This article is licensed under a Creative Commons Attribution-NonCommercial 3.0 Unported Licence.

44 B. L. Tran, H.-Y. Chin, B. K. Chang and A. S. T. Chiang, *Microporous Mesoporous Mater.*, 2019, **277**, 149–153.
45 N. Zhong, X. Ren, L. Cheng, M. Yamamoto, T. Leskinen, J. Lommi, H. Zhu, T. Granstrom, J. Saddler and X. Bi, *Energy Convers. Manag.*, 2023, **295**, 117620.
46 S. Allende, G. Brodie and M. V. Jacob, *Environ. Res.*, 2023, **226**, 115619.
47 R. Potnuri, D. V. Surya, C. S. Rao, A. Yadav, V. Sridevi and N. Remya, *J. Anal. Appl. Pyrolysis*, 2023, **173**, 106094.
48 J. Vermeiren, N. Dilissen, V. Goovaerts and J. Vleugels, *Constr. Build. Mater.*, 2024, **428**, 136271.
49 P. Guzik, P. Kulawik, M. Zając and W. Migdał, *Crit. Rev. Food Sci. Nutr.*, 2022, **62**, 7989–8008.
50 A. Kumar, Y. Kuang, Z. Liang and X. Sun, *Mater. Today Nano*, 2020, **11**, 100076.
51 N. Devi, S. Sahoo, R. Kumar and R. K. Singh, *Nanoscale*, 2021, **13**, 11679–11711.
52 S. Kumar N, D. Grekov, P. Pré and B. J. Alappat, *Renew. Sustain. Energy Rev.*, 2020, **124**, 109743.
53 J. Letwaba, U. O. Uyor, M. L. Mavhungu, N. O. Achuka and P. A. Popoola, *RSC Adv.*, 2024, **14**, 14233–14253.
54 F. Zhang, T. Zhou, Y. Liu and J. Leng, *Sci. Rep.*, 2015, **5**, 11152.
55 Z. Zhao, H. Li, K. Zhao, L. Wang and X. Gao, *Chem. Eng. J.*, 2022, **428**, 131006.
56 T. V. Tran, A. A. Jalil, D. T. C. Nguyen, M. Alhassan, W. Nabgan, A. N. T. Cao, T. M. Nguyen and D.-V. N. Vo, *Environ. Res.*, 2023, **216**, 114422.
57 M. Taheri, I. Di Bernardo, A. Lowe, D. R. Nisbet and T. Tsuzuki, *Cryst. Growth Des.*, 2020, **20**, 2761–2773.
58 W. Xu, H. Chen, K. Jie, Z. Yang, T. Li and S. Dai, *Angew. Chem., Int. Ed.*, 2019, **58**, 5018–5022.
59 S. Głowniak, B. Szczęśniak, J. Choma and M. Jaroniec, *Mater. Today*, 2021, **46**, 109–124.
60 T.-H. Wei, S.-H. Wu, Y.-D. Huang, W.-S. Lo, B. P. Williams, S.-Y. Chen, H.-C. Yang, Y.-S. Hsu, Z.-Y. Lin, X.-H. Chen, P.-E. Kuo, L.-Y. Chou, C.-K. Tsung and F.-K. Shieh, *Nat. Commun.*, 2019, **10**, 5002.
61 D. Kim, J. Park, J. Park, J. Jang, M. Han, S. Lim, D. Y. Ryu, J. You, W. Zhu, Y. Yamauchi and J. Kim, *Small Methods*, 2024, **8**, 2400236.
62 A. Deacon, L. Briquet, M. Malankowska, F. Massingberd-Mundy, S. Rudić, T. l. Hyde, H. Cavaye, J. Coronas, S. Poulston and T. Johnson, *Commun. Chem.*, 2022, **5**, 18.
63 B. Zheng, L. L. Wang, J. C. Hui, L. Du, H. Du and M. Zhu, *Dalton Trans.*, 2016, **45**, 4346–4351.
64 T. Yu, Q. Cai, G. Lian, Y. Bai, X. Zhang, X. Zhang, L. Liu and S. Zhang, *Chem. Eng. J.*, 2021, **419**, 129638.
65 Z. Zhang, Y. Chen, C. Hu, C. Zuo, P. Wang, W. Chen and T. Ao, *Environ. Res.*, 2021, **198**, 111254.
66 L. Q. Phan, T. T. T. Nguyen, D. T. C. Nguyen and T. V. Tran, *Surf. Interfaces*, 2024, **46**, 103995.
67 A. A. Tezerjani, R. Halladj and S. Askari, *RSC Adv.*, 2021, **11**, 19914–19923.
68 E. Santoso, R. Ediati, Z. Istiqomah, D. O. Sulistiono, R. E. Nugraha, Y. Kusumawati, H. Bahruji and D. Prasetyoko, *Microporous Mesoporous Mater.*, 2021, **310**, 110620.
69 Y. N. Wu, M. Zhou, B. Zhang, B. Wu, J. Li, J. Qiao, X. Guan and F. Li, *Nanoscale*, 2014, **6**, 1105–1112.
70 T. V. Tran, H. Nguyen, P. H. A. Le, D. T. C. Nguyen, T. T. Nguyen, C. V. Nguyen, D.-V. N. Vo and T. D. Nguyen, *J. Environ. Chem. Eng.*, 2020, **8**, 104189.
71 M. I. Ostad, M. N. Shahrak and F. Galli, *Microporous Mesoporous Mater.*, 2021, **326**, 111363.
72 J. A. Allegretto, D. Onna, S. A. Bilmes, O. Azzaroni and M. Rafti, *Chem. Mater.*, 2024, **36**, 5814–5825.
73 M. G. Moustafa, A. M. Aboraia, V. V. Butova, F. Elmasry and A. A. Guda, *New J. Chem.*, 2022, **46**, 9138–9145.
74 P. D. Du, N. T. Hieu and T. V. Thien, *J. Nanomater.*, 2021, **2021**, 1–12.
75 Y.-R. Lee, M.-S. Jang, H.-Y. Cho, H.-J. Kwon, S. Kim and W.-S. Ahn, *Chem. Eng. J.*, 2015, **271**, 276–280.
76 N. Ahmad, A. Samavati, N. A. H. M. Nordin, J. Jaafar, A. F. Ismail and N. A. N. N. Malek, *Sep. Purif. Technol.*, 2020, **239**, 116554.
77 Z. Pei, P. Fei, A. Zhang, J. Guo, J. Hao, J. Jia, H. Dong, Q. Shen, L. Wei, H. Jia and B. Xu, *J. Alloys Compd.*, 2022, **904**, 164055.
78 C. Zhang, Z. Shu, H. Sun, L. Yan, C. Peng, Z. Dai, L. Yang, L. Fan and Y. Chu, *Appl. Surf. Sci.*, 2023, **611**, 155599.
79 Y. Yang, Z. Guo, W. Huang, S. Zhang, J. Huang, H. Yang, Y. Zhou, W. Xu and S. Gu, *Appl. Surf. Sci.*, 2020, **503**, 144079.
80 X. Xia, X. Song, Y. Li, W. Hou, H. Lv, F. Li, Y. Li, J. Liu and X. Li, *Front. Bioeng. Biotechnol.*, 2022, **10**, 1026743.
81 P. Gao, Y. Chen, W. Pan, N. Li, Z. Liu and B. Tang, *Angew. Chem.*, 2021, **133**, 16901–16914.
82 H. Xie, X. Liu, Z. Huang, L. Xu, R. Bai, F. He, M. Wang, L. Han, Z. Bao, Y. Wu, C. Xie and Y. Gong, *Cancers*, 2022, **14**, 3935.
83 C. Hu, Y. Yu, S. Chao, H. Zhu, Y. Pei, L. Chen and Z. Pei, *Molecules*, 2021, **26**, 3878.
84 Z. Xie, S. Liang, X. Cai, B. Ding, S. Huang, Z. Hou, P. Ma, Z. Cheng and J. Lin, *ACS Appl. Mater. Interfaces*, 2019, **11**, 31671–31680.
85 L. Gao, Z. Wu, A.-R. Ibrahim, S.-F. Zhou and G. Zhan, *ACS Biomater. Sci. Eng.*, 2020, **6**, 6095–6107.
86 Y. C. Ma, Y. H. Zhu, X. F. Tang, L. F. Hang, W. Jiang, M. Li, M. I. Khan, Y. Z. You and Y. C. Wang, *Biomater. Sci.*, 2019, **7**, 2740–2748.
87 P. S. Maharjan and H. K. Bhattarai, *J. Oncol.*, 2022, **2022**, 1–20.
88 C. Li, J. Ye, X. Yang, S. Liu, Z. Zhang, J. Wang, K. Zhang, J. Xu, Y. Fu and P. Yang, *ACS Nano*, 2022, **16**, 18143–18156.
89 S. Chen, Y. Xie, X. Guo and D. Sun, *Microchem. J.*, 2022, **181**, 107715.
90 S. Yao, X. Zhao, L. Wang, F. Chen, H. Gong, C. Chen and C. Cai, *Microchim. Acta*, 2022, **189**, 266.
91 S. Zhang, F. Rong, C. Guo, F. Duan, L. He, M. Wang, Z. Zhang, M. Kang and M. Du, *Coord. Chem. Rev.*, 2021, **439**, 213948.
92 L. Meng, K. Xiao, X. Zhang, C. Du and J. Chen, *Biosens. Bioelectron.*, 2020, **150**, 111861.

Open Access Article. Published on 27 Mei 2025. Downloaded on 02/06/2026 13:51:38.
This article is licensed under a Creative Commons Attribution-NonCommercial 3.0 Unported Licence.

93 S. Roy, A. Mathur and A. Bihari Pati, *Electroanalysis*, 2023, **35**, e202200203.
94 L. Kong, S. Lv, Z. Qiao, Y. Yan, J. Zhang and S. Bi, *Biosens. Bioelectron.*, 2022, **207**, 114188.
95 L. A. Stamp, E. Lei, J. J. M. Liew, R. V. Pustovit, M. M. Hao, D. H. Croaker, J. B. Furness and C. D. Adams, *Biol. Methods Protoc.*, 2022, **7**, bpac004.
96 Y. Zhang, N. Li, Y. Xu, M. Yang, X. Luo, C. Hou and D. Huo, *Microchem. J.*, 2023, **187**, 108316.
97 P. Kushwaha and P. Chauhan, *Magn. Reson. Imaging*, 2023, **95**, 50–58.
98 Y. B. Pan, A. Shao, J. Zhang, S. Wang, X. He, W. Tang, J. Wang and S. Wang, *J. Mater. Chem. B*, 2019, **7**, 7683–7689.
99 H. Guo, Y. Xia, K. Feng, X. Qu, C. Zhang and F. Wan, *Int. J. Nanomed.*, 2020, **15**, 3235–3250.
100 W. Zhou, J. Shen, J. Lin, M. An, L. An, Q. Tian and S. Yang, *J. Mater. Sci.*, 2021, **56**, 7386–7396.
101 P. Pandit, S. Bhagat, P. Rananaware, Z. Mohanta, M. Kumar, V. Tiwari, S. Singh and V. P. Brahmkhatri, *Microporous Mesoporous Mater.*, 2022, **340**, 112008.
102 Z. Zhou, M. Vázquez-González and I. Willner, *Chem. Soc. Rev.*, 2021, **50**, 4541–4563.
103 Z. Lei, Q. Tang, Y. Ju, Y. Lin, X. Bai, H. Luo and Z. Tong, *J. Biomater. Sci. Polym. Ed.*, 2020, **31**, 695–711.
104 J. Yan, C. Liu, Q. Wu, J. Zhou, X. Xu, L. Zhang, D. Wang, F. Yang and H. Zhang, *Anal. Chem.*, 2020, **92**, 11453–11461.
105 W. Zhu, W. Huang, L. Ye, Y. Deng, Q. Xie and Y. Jiang, *Chem. Eng. Sci.*, 2020, **228**, 115981.
106 X. Mi, M. Hu, M. Dong, Z. Yang, X. Zhan, X. Chang, J. Lu and X. Chen, *Int. J. Nanomed.*, 2021, **16**, 8337–8352.
107 Z. Yin, M. Lin, Y. Xu, Z. Wang, Y. Cai and X. Yang, *Mater. Lett.*, 2021, **301**, 130276.
108 A. Stahl and Y. P. Yang, *Tissue Eng. Part B Rev.*, 2021, **27**, 539–547.
109 E. Issaka, J. N. O. Amu-Darko, M. Adams, S. Yakubu, E. Gyimah, N. Ali, J. Cui and M. Bilal, *Top. Catal.*, 2023, **153**, 2083–2106.
110 Y. Hou, R. Zhang, H. Cheng, Y. Wang, Q. Zhang, L. Zhang, L. Wang, R. Li, X. Wu and B. Li, *Colloids Surf., A*, 2023, **656**, 130264.
111 B. Tao, W. Zhao, C. Lin, Z. Yuan, Y. He, L. Lu, M. Chen, Y. Ding, Y. Yang, Z. Xia and K. Cai, *Chem. Eng. J.*, 2020, **390**, 124621.
112 M. Qiao, Z. Xu, X. Pei, Y. Liu, J. Wang, J. Chen, Z. Zhu and Q. Wan, *Chem. Eng. J.*, 2022, **434**, 134583.
113 M. A. Al-Baadani, L. Xu, K. H. R. Yie, A. Sun, X. Gao, K. Cai, B. A. Al-Shaaobi, A. M. Al-Bishari, L. Cai, X. Shen, J. Liu and P. Ma, *Mater. Des.*, 2022, **217**, 110596.
114 X. Zhang, J. Chen, X. Pei, Y. Li, H. Feng, Z. He, W. Xie, X. Pei, Z. Zhu, Q. Wan and J. Wang, *Adv. Healthc. Mater.*, 2023, **12**, 2202317.
115 Y. Liu, Z. Zhu, X. Pei, X. Zhang, X. Cheng, S. Hu, X. Gao, J. Wang, J. Chen and Q. Wan, *ACS Appl. Mater. Interfaces*, 2020, **12**, 36978–36995.
116 F. Zou, J. Jiang, F. Lv, X. Xia and X. Ma, *NanoBiotechnology*, 2020, **18**, 39.
117 C. Yang, J. Wen, Z. Xue, X. Yin, Y. Li and L. Yuan, *J. Environ. Sci.*, 2023, **127**, 91–101.

© 2025 The Author(s). Published by the Royal Society of Chemistry